PHYSICAL REVIEW D **89,** 085032 (2014)

Renormalization group analysis of the gluon mass equation

A. C. Aguilar,[1] D. Binosi,[2] and J. Papavassiliou[3]

[1]*Institute of Physics "Gleb Wataghin," University of Campinas—UNICAMP, 13083-859 Campinas, São Paulo, Brazil*

[2]*European Centre for Theoretical Studies in Nuclear Physics and Related Areas (ECT*) and Fondazione Bruno Kessler, Villa Tambosi, Strada delle Tabarelle 286, I-38123 Villazzano Trento, Italy*

[3]*Department of Theoretical Physics and IFIC, University of Valencia and CSIC, E-46100 Valencia, Spain*

(Received 22 January 2014; published 18 April 2014)

We carry out a systematic study of the renormalization properties of the integral equation that determines the momentum evolution of the effective gluon mass in pure Yang–Mills theory, without quark effects taken into account. A detailed, all-order analysis of the complete kernel appearing in this particular equation, derived in the Landau gauge, reveals that the renormalization procedure may be accomplished through the sole use of ingredients known from the standard perturbative treatment of the theory, with no additional assumptions. However, the subtle interplay of terms operating at the level of the exact equation gets distorted by the approximations usually employed when evaluating the aforementioned kernel. This fact is reflected in the form of the obtained solutions, for which the deviations from the correct behavior are best quantified by resorting to appropriately defined renormalization-group invariant quantities. This analysis, in turn, provides a solid guiding principle for improving the form of the kernel, and furnishes a well-defined criterion for discriminating between various possibilities. Certain renormalization-group inspired Ansätze for the kernel are then proposed, and their numerical implications are explored in detail. One of the solutions obtained fulfills the theoretical expectations to a high degree of accuracy, yielding a gluon mass that is positive definite throughout the entire range of physical momenta, and displays in the ultraviolet the so-called "power-law" running, in agreement with standard arguments based on the operator product expansion. Some of the technical difficulties thwarting a more rigorous determination of the kernel are discussed, and possible future directions are briefly mentioned.

DOI: 10.1103/PhysRevD.89.085032 PACS numbers: 12.38.Aw, 12.38.Lg, 14.70.Dj

I. INTRODUCTION

A recent development in the ongoing study of the basic QCD Green's functions within the nonperturbative framework of the Schwinger–Dyson equations (SDEs) [1–18] is the derivation of the particular integral equation that governs the momentum evolution of the effective gluon mass [19–22]. As has been argued in a series of works [23–26], the generation of such a mass offers a natural and self-consistent explanation for the infrared finiteness of the (Landau gauge) gluon propagator and ghost dressing function [11,19,20,27,28], established in large-volume (quenched) lattice simulations, both in $SU(2)$ [29] and in $SU(3)$ [30,31], as well as in full QCD simulations [32,33] on moderate-size lattices.

The systematic scrutiny of this equation could eventually place the gluon mass generation on an equal conceptual footing as the more familiar phenomenon of constituent quark mass generation [1,34–38]. To reach an equivalent level of understanding, however, several theoretical tasks need be carried out. In particular, one of the main unresolved issues in this context is the proper renormalization of this homogeneous integral equation. The renormalization procedure, in turn, may impose crucial restrictions on the form of its kernel, which, even though it is formally known, for all practical purposes must undergo approximations and modelling [21].

In the present work, we study in detail the general renormalization procedure and, most importantly, the properties of the mass equation, and its corresponding solutions, under the renormalization group (RG). This is a rather technical endeavor, for which the main field-theoretic points may be summarized as follows.

To begin with, it is important to recognize that the renormalization of the mass equation, as well as the gluon mass itself, is accomplished entirely by means of the same renormalization constants familiar from the perturbative treatment of Yang–Mills theories, namely, those associated with the gluon and ghost propagators, and the various interaction vertices [39]. The deeper field-theoretic reasons for this fact may be traced back to the intricate dynamical mechanism that generates this effective mass; specifically, the formation of nonperturbative massless bound states [40–44], which act as would-be Goldstone bosons, trigger the well-known Schwinger mechanism [45,46], without ever modifying the original Lagrangian. In addition, a crucial identity enforces the total annihilation of any potential quadratic divergence, related to seagull-type integrals [47]. As a result, no bare gluon mass needs be

introduced at any stage; this is absolutely essential, since a term of the type $m_0^2 A_\mu^2$ is forbidden by the local gauge invariance of the Yang–Mills Lagrangian [10,19].

Furthermore, it is clear that the correct implementation of the aforementioned renormalization procedure relies crucially on the precise properties of the kernel of the mass equation under the RG. If the kernel is treated at the formal level, these properties are automatically enforced, as a direct consequence of the corresponding RG properties of the basic ingredients that build it up. However, the kernel is expressed in terms of a complicated diagrammatic expansion, which, for all practical purposes, must be truncated, and further simplified or approximated [21]. As a result, the exact RG properties of the kernel may be compromised; this flaw, in turn, will make its way into the solutions obtained from the corresponding mass equation. Thus, depending on the quality of the approximations employed for the kernel, the corresponding gluon masses will encode their formal RG properties with variable degrees of accuracy.

The quantitative study of the situation described above may be best accomplished by using RG-invariant (RGI) quantities, which, by construction, maintain the same form before and after renormalization, and are independent of the value of the renormalization point μ, used to implement the various subtractions [19,27]. In particular, a RGI gluon mass may be defined, and then subsequently constructed from the solutions of the mass equation, for any given Ansatz for the kernel, and for several different values of μ. Then, the amount by which the resulting quantity departs from the perfect μ independence can serve as a discriminant of the various possible Ansätze for the kernel.

Let us finally emphasize for completeness that our entire analysis is carried out within the pure $SU(3)$ Yang–Mills theory, with no quark effects included, and that throughout the present work we employ the standard Landau gauge.

The article is organized as follows. In Sec. II we introduce the relevant notation, define the basic renormalization constants, and discuss in detail the particularities of the gluon mass and its renormalization. In Sec. III we carry out the full renormalization of the gluon mass equation and explore its properties under the RG. Then, in Sec. IV we study the tensorial structure of the main unknown ingredient that composes the kernel and determine how its various form factors affect the infrared behavior of the mass equation. In Sec. V we outline the procedure for estimating the discrepancies from the correct RG behavior induced by the various approximations to the kernel. This procedure is then applied to the original version of the mass equation, and considerable deviations are found. In Sec. VI we present two RG-inspired improvements of the kernel, which, *a priori*, seem to capture more faithfully its formal RG properties, and determine the corresponding departures of the new solutions from the ideal μ independence. This study reveals a significant improvement, in accordance with the initial expectation. The asymptotic behavior of one of these "improved"solutions is further analyzed, suggesting a possible connection with general arguments originating from the operator product expansion (OPE) [48–50]. Finally, in Sec. VII we present our discussion and conclusions.

II. RENORMALIZATION AND THE GLUON MASS

In this section we set up the notation and introduce the field theoretic relations and concepts necessary for carrying out the renormalization of the gluon mass equation and for exploring its properties under the RG.

A. General renormalization relations

In the Landau gauge, the full gluon propagator (quenched or unquenched) assumes the general form

$$i\Delta_{\mu\nu}(q) = -i\Delta(q^2)P_{\mu\nu}(q); \qquad P_{\mu\nu}(q) = g_{\mu\nu} - q_\mu q_\nu/q^2. \tag{2.1}$$

At any finite order in perturbation theory, the scalar cofactor $\Delta(q^2)$ is conveniently parametrized in terms of the *inverse* gluon dressing function, $J(q^2)$,

$$\Delta^{-1}(q^2) = q^2 J(q^2). \tag{2.2}$$

In addition, the full ghost propagator, $D(q^2)$, is usually parametrized in terms of the corresponding ghost dressing function, $F(q^2)$, according to

$$D(q^2) = \frac{F(q^2)}{q^2}. \tag{2.3}$$

We will now consider the combination of the pinch technique (PT) [19,51–55] with the background field method (BFM) [56], known as the PT-BFM scheme [10,57,58]. Within the PT-BFM formalism, the natural separation of the gluonic field into a "quantum" (Q) and a "background" (B) part gives rise to an increase in the type of possible Green's functions that one may consider [56]. In particular, three types of gluon propagators make their appearance: (i) the conventional gluon propagator (two quantum gluons entering, QQ), denoted (as above) by $\Delta(q^2)$; (ii) the background gluon propagator (two background gluons entering, BB), indicated by $\hat{\Delta}(q^2)$; and (iii) the mixed background-quantum gluon propagator (one background and one quantum gluons entering, BQ), denoted by $\tilde{\Delta}(q^2)$.

The conversion between quantum and background two-point functions is achieved through the so-called background-quantum identities (BQIs) [59,60]. For instance, $\hat{\Delta}$ and Δ, as well as their corresponding components, are related by

$$\hat{O}(q^2) = [1 + G(q^2)]^2 O(q^2); \qquad O = \Delta^{-1}, J, m^2,$$
$$\tilde{O}(q^2) = [1 + G(q^2)] O(q^2). \tag{2.4}$$

The function $G(q^2)$ represents the $g_{\mu\nu}$ component of a special Green's function, $\Lambda_{\mu\nu}(q)$, typical of the PT-BFM framework [53], i.e., $\Lambda_{\mu\nu}(q) = G(q^2) g_{\mu\nu} + L(q^2) q_\mu q_\nu / q^2$; for various field-theoretic properties of the above functions, see Ref. [61] and references therein. Here it should suffice to mention that, for practical purposes, one often uses the approximate (but rather accurate) relation

$$1 + G(q^2) \approx F^{-1}(q^2), \tag{2.5}$$

which becomes exact in the deep IR [27,61–63].

At any finite order in perturbation theory, the renormalization of the pure Yang–Mills theory proceeds through the standard redefinition of the bare fundamental fields, gluon $A_0^{a\mu}(x)$, ghost $c_0^a(x)$, and the bare gauge coupling, g_0; specifically, the corresponding renormalized quantities, $A_R^{a\mu}(x)$, $c_R^a(x)$, and g_R, are given by

$$A_R^{a\mu}(x) = Z_A^{-1/2} A_0^{a\mu}(x), \qquad c_R^a(x) = Z_c^{-1/2} c_0^a(x);$$
$$g_R = Z_g^{-1} g_0. \tag{2.6}$$

Then the associated two-point functions are renormalized as

$$\Delta_R(q^2) = Z_A^{-1} \Delta_0(q^2); \qquad D_R(q^2) = Z_c^{-1} D_0(q^2), \tag{2.7}$$

or, equivalently,

$$J_R(q^2) = Z_A J_0(q^2); \qquad F_R(q^2) = Z_c^{-1} F_0(q^2). \tag{2.8}$$

Similarly, the renormalization constants of the three fundamental Yang–Mills vertices (gluon-ghost, three-gluon, and four-gluon vertices) are defined as [64]

$$\Gamma_R^{\mu} = Z_1 \Gamma_0^{\mu}; \qquad \Gamma_R^{\mu\alpha\beta} = Z_3 \Gamma_0^{\mu\alpha\beta}; \qquad \Gamma_R^{\mu\alpha\beta\nu} = Z_4 \Gamma_0^{\mu\alpha\beta\nu}. \tag{2.9}$$

The standard Slavnov–Taylor identities (STIs) of the theory enforce a set of important relations on the various renormalization constants [64], namely,

$$Z_g = Z_1 Z_A^{-1/2} Z_c^{-1} = Z_3 Z_A^{-3/2} = Z_4^{1/2} Z_A^{-1}, \tag{2.10}$$

which will be used extensively in Sec. III.

In the BFM one introduces, in addition, the wave-function renormalization constant $\hat{Z}_A$, associated with the background gluon B. Then, $\hat{\Delta}(q^2)$ renormalizes according to

$$\hat{\Delta}_R(q^2) = \hat{Z}_A^{-1} \hat{\Delta}_0(q^2). \tag{2.11}$$

Because of the Abelian Ward identities (WIs) of the BFM, Z_g and $\hat{Z}_A$ are related by the fundamental QED-like relation [56]

$$Z_g = \hat{Z}_A^{-1/2}. \tag{2.12}$$

Finally, the renormalization relation for $G(q^2)$ reads [61]

$$1 + G_R(q^2) = Z_G [1 + G_0(q^2)], \tag{2.13}$$

where, due to Eqs. (2.4) and (2.12), $Z_G = \hat{Z}_A^{1/2} Z_A^{-1/2} = Z_g^{-1} Z_A^{-1/2}$.

B. Gluon mass renormalization

Nonperturbatively, the dynamical generation of an effective gluon mass accounts for the infrared finiteness of the (Landau gauge) gluon propagator, observed in a variety of large-volume lattice simulations [29–32]. To describe this behavior, the parametrization in Eq. (2.2) is modified according to (Minkowski space) [20]

$$\Delta^{-1}(q^2) = q^2 J(q^2) - m^2(q^2), \tag{2.14}$$

with $m^2(0) \neq 0$. In addition, the generation of the aforementioned mass explains also, in a natural way, the corresponding saturation of the ghost dressing function, $F(q^2)$ [4,11]. Moreover, both $\hat{\Delta}(q^2)$ and $\tilde{\Delta}(q^2)$ are also infrared finite and must be parametrized in a way exactly analogous to that of $\Delta(q^2)$ in Eq. (2.14), namely, in terms of $\hat{J}(q^2)$, $\hat{m}^2(q^2)$ and $\tilde{J}(q^2)$, $\tilde{m}^2(q^2)$, respectively [21].

It is important to emphasize that the generation of a gluon mass does not interfere, in any way, with the renormalization of the theory, which proceeds exactly as before. In particular, the following main points must be stressed:

(i) The Lagrangian of the Yang–Mills theory (or that of QCD) is never altered; the generation of the gluon mass takes place dynamically, without violating any of the underlying symmetries. In particular, no bare gluon mass is introduced, since a term of the type $m_0^2 A_\mu^2$ is forbidden by the local gauge invariance. However, although no such term is *ab initio* introduced, the possible appearance of the so-called "seagull" divergences at later stages of the analysis could force its emergence. Such divergences are produced by integrals of the type $\int_k \Delta(k)$ or variations thereof [47]; in dimensional regularization they give rise to terms of the type $m_0^2(1/\epsilon)$, while, in the case of a hard cutoff Λ, they correspond to terms proportional to Λ^2 (quadratic divergences). Evidently, their disposal would require the introduction in the original Lagrangian of a counterterm of the form $m_0^2 A_\mu^2$, which would be violating the basic assumptions stated above. Nonetheless, it turns out

that, due to a set of subtle relations, particular to the PT-BFM framework, all such divergences are completely canceled [47].

(ii) Even though there is no "bare gluon mass," in the sense explained above, the momentum-dependent $m^2(q^2)$ undergoes renormalization, which, however, is not associated with a new renormalization constant but is implemented by the (already existing) wave-function renormalization constant of the gluon, namely, Z_A. Specifically, from Eq. (2.14), and given that $\Delta^{-1}(0) = m^2(0)$, we have that the gluon masses before and after renormalization are related by

$$m_R^2(q^2) = Z_A m_0^2(q^2). \tag{2.15}$$

(iii) The above renormalization condition is fully consistent with (and may be independently derived from) the general procedure that implements the gauge-invariant (i.e., STI-preserving) generation of a gluon mass. Specifically, within the PT-BFM framework, the fully dressed vertex BQ^2, before mass generation, satisfies the WI [55]

$$q^\alpha \tilde{\Gamma}_{\alpha\mu\nu}(q,r,p) = p^2 J(p^2) P_{\mu\nu}(p) - r^2 J(r^2) P_{\mu\nu}(r), \tag{2.16}$$

and, given the first relation in Eq. (2.8), the corresponding vertex renormalization constant, $\tilde{Z}_3$, must obey

$$\tilde{Z}_3 = Z_A. \tag{2.17}$$

Then, for gauge invariance to be preserved, one must modify this vertex according to [20]

$$\tilde{\Gamma}'_{\alpha\mu\nu}(q,r,p) = [\tilde{\Gamma}(q,r,p) + \tilde{V}(q,r,p)]_{\alpha\mu\nu}, \tag{2.18}$$

where the special vertex $\tilde{V}(q,r,p)$ is completely longitudinal, i.e.,

$$P^{\alpha'\alpha}(q) P^{\mu'\mu}(r) P^{\nu'\nu}(p) \tilde{V}_{\alpha\mu\nu}(q,r,p) = 0, \tag{2.19}$$

and contains massless poles of purely nonperturbative origin [40–44], which will be ultimately responsible for triggering the well-known Schwinger mechanism [45,46]. Now, $\tilde{\Gamma}$ and $\tilde{\Gamma}'_{\alpha\mu\nu}$ must be renormalized by $\tilde{Z}_3$, and so

$$\tilde{V}_R^{\alpha\mu\nu}(q,r,p) = Z_A \tilde{V}_0^{\alpha\mu\nu}(q,r,p). \tag{2.20}$$

Since, in order for the WIs to remain intact, $\tilde{V}_{\alpha\mu\nu}$ must satisfy

$$q^\alpha \tilde{V}_{\alpha\mu\nu}(q,r,p) = m^2(r^2) P_{\mu\nu}(r) - m^2(p^2) P_{\mu\nu}(p), \tag{2.21}$$

one finally concludes that Eq. (2.15) must be fulfilled.

(iv) We emphasize that the "mass renormalization" introduced above is not associated with a counterterm of the type $\delta m^2 = m_R^2 - m_0^2$, as is typical in the case of hard boson masses, such as in scalar theories, or the electroweak sector of the Standard Model. Instead, it is akin to the renormalization that higher-order Green's functions must undergo, in order to be made finite, even though no individual counterterm is assigned to them.

Consider, for instance, a scalar ϕ^4 theory (in $d = 4$), and the (one-particle irreducible) n-point functions, $G^{(n)}(p_i)$ with $n \geq 5$. It is well known that any such function ought to be made finite by means of the renormalization constants already defined for $n \leq 5$, since no counterterms of the form ϕ^n (with $n \geq 5$) are allowed [64]. Indeed, $G^{(n)}(p_i)$ can be made finite by expressing the bare mass and coupling constant (μ_0, λ_0) in terms of their renormalized counterparts (μ_R, λ_R) and then multiplying by $Z_\phi^{1/2}$ for each external leg, i.e., $G_R^{(n)}(p_i, \mu_R, \lambda_R) = Z_\phi^{n/2} G_0^{(n)}(p_i, \mu_0, \lambda_0)$.

A similar situation arises when considering the gluon mass within the so-called "massless bound-state formalism" [65,66], where one focuses on the details of the nonperturbative formation of the pole vertex mentioned in (iii). Specifically, the relevant vertex part, denoted by $\mathcal{U}_{\alpha\mu\nu}$ (see Fig. 1), has the form

$$\mathcal{U}_{\alpha\mu\nu}(q,r,p) = I_\alpha(q) \left(\frac{i}{q^2}\right) B_{\mu\nu}(q,r,p), \tag{2.22}$$

where $I_\alpha(q)$ represents the transition amplitude that mixes a quantum gluon with the massless excitation, i/q^2 corresponds to the propagator of the massless excitation, and B is an effective vertex describing the interaction between the massless excitation and gluons. Obviously, Lorentz invariance dictates that $I_\alpha(q) = q_\alpha I(q^2)$. In addition [66],

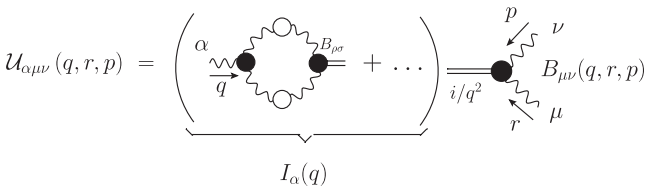

FIG. 1. The vertex $U_{\alpha\mu\nu}$ is composed of three main ingredients: the transition amplitude, $I_\alpha(q)$, which mixes the gluon with a massless excitation; the propagator of the massless excitation i/q^2; and the massless excitation gluon vertex $B_{\mu\nu}$. The omitted terms are not relevant for this analysis; they can be found in Refs. [65,66].

$$I_\alpha(q) = \int_k \Gamma_{\alpha\mu\nu}\Delta^{\mu\sigma}(k+q)\Delta^{\nu\rho}(k)B_{\rho\sigma} + \cdots, \quad (2.23)$$

where the ellipses indicate the graphs omitted in Fig. 1 (see Ref. [65] for the complete version); the inclusion of these diagrams does not modify the basic argument, but it simply makes it lengthier. In the equations above, we have introduced the dimensional regularization measure $\int_k = \mu^\epsilon \int d^dk/(2\pi)^d$, where $d = 4-\epsilon$ is the space-time dimension and μ the 't Hooft mass.

We now renormalize the effective vertex B by introducing the renormalization constant Z_B,

$$B_R^{\rho\sigma} = Z_B^{-1} B_0^{\rho\sigma}, \quad (2.24)$$

and combine Eqs. (2.22) and (2.23). Since $\mathcal{U}$ forms part of the three-gluon vertex (of the type Q^3), it renormalizes as $\mathcal{U}_R^{\mu\alpha\beta} = Z_3 \mathcal{U}_0^{\mu\alpha\beta}$, and with the help of Eqs. (2.7) and (2.9), one concludes that (note that the dependence of U on B is effectively quadratic)

$$Z_B = Z_A^{-1}. \quad (2.25)$$

With these ingredients at hand, we now turn to the basic formula relating the gluon mass with the transition amplitude [65,66], namely,

$$m(q^2) = gI(q^2). \quad (2.26)$$

Let us consider Eq. (2.26) written in terms of unrenormalized quantities and substitute in its rhs the corresponding renormalized ones, by introducing the appropriate renormalization constants. Suppressing Lorentz indices and using $Z_g = Z_3 Z_A^{-3/2}$ [see Eq. (2.10)], one finds

$$m_0(q^2) = Z_A^{-1/2} g_R \int_k \Gamma_R \Delta_R(k+q)\Delta_R(k)B_R, \quad (2.27)$$

which clearly requires the renormalization dictated by Eq. (2.15) in order to be converted into the manifestly renormalized form

$$m_R(q^2) = g_R I_R(q^2). \quad (2.28)$$

C. Basic RGI quantities

Let us finally consider certain RGI combinations of Green's functions, which will be useful in the ensuing analysis. We recall that, by definition, a RGI combination maintains exactly the same form when written in terms of unrenormalized or renormalized quantities.

To begin with, as is well known and easy to verify directly using Eq. (2.12), the combination [27,63]

$$d(q^2) = g^2\hat{\Delta}(q^2) = \frac{g^2\Delta(q^2)}{[1+G(q^2)]^2} \quad (2.29)$$

is an RGI quantity [note that in the second equality the BQI of Eq. (2.4) was employed]. It is then natural to *define* a RGI gluon mass, to be denoted by $\bar{m}(q^2)$ [21], as

$$\bar{m}^2(q^2) = g^{-2}\hat{m}^2(q^2) = g^{-2}[1+G(q^2)]^2 m^2(q^2). \quad (2.30)$$

We emphasize that the $\bar{m}^2(q^2)$ defined above is a convenient quantity to introduce because, as will become apparent in the rest of this work, it helps us quantify the faithfulness of certain approximations with respect to the RG. Note, however, that no special physical meaning is ascribed to $\bar{m}(q^2)$ at this stage; in particular, despite its RGI nature, we explicitly refrain from promoting it to a physical observable, for the simple reason that, at least within our present understanding, it is a quantity that depends on the gauge-fixing parameter. Specifically, all recent work related to the gluon mass equation has been performed in the Landau gauge, mainly because the corresponding lattice simulations have been carried out in this privileged gauge. In fact, the question whether the gluon propagator continues to saturate in the infrared when computed away from the Landau gauge is practically unexplored, both on the lattice as well as within the SDE framework.

We finally point out that the definition of the RGI gluon mass introduced here differs from the alternative proposed in Ref. [67], namely, $\bar{m}^2(q^2) = m^2(q^2)J^{-1}(q^2)$. The problem with this latter definition is that, while formally RGI, it gives rise to an ill-defined expression, due to the singular behavior of the quantity $J(q^2)$. Specifically, the contribution of the massless ghost loop forces $J(q^2)$ to reverse its sign and finally diverge logarithmically in the deep infrared [68]; of course, the combination $q^2J(q^2)$, appearing in the definition of $\Delta^{-1}(q^2)$ [see Eq. (2.14)], is perfectly finite.

Let us next introduce three additional RGI quantities, to be generically denoted by $\mathcal{R}_i$, formed out of special combinations of propagators, vertices, and the gauge coupling constant. In particular, we define

$$\begin{aligned}
\mathcal{R}_1^{\mu\alpha\beta}(q,r,p) &= g\Delta^{1/2}(q)\Delta^{1/2}(r)\Delta^{1/2}(p)\Gamma^{\mu\alpha\beta}(q,r,p),\\
\mathcal{R}_2^{\mu}(q,r,p) &= g\Delta^{1/2}(q)^{1/2}(r)D^{1/2}(p)\Gamma^{\mu}(q,r,p),\\
\mathcal{R}_3^{\mu\alpha\beta\nu}(q,r,p,s) &= g^2\Delta^{1/2}(q)\Delta^{1/2}(r)\Delta^{1/2}(p)\Delta^{1/2}(s)\\
&\quad\times\Gamma^{\mu\alpha\beta\nu}(q,r,p,s).
\end{aligned} \quad (2.31)$$

The RGI nature of the above quantities may be verified directly, by employing the relations listed in Eq. (2.10).

III. RG PROPERTIES OF THE FULL GLUON MASS EQUATION

In this section we study the RG structure of the integral equation that controls the momentum evolution of the gluon mass. The main result of this analysis is that the *complete* kernel of this equation acquires a form that allows

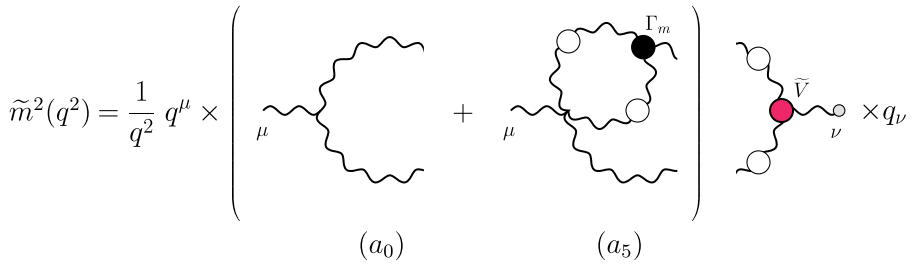

FIG. 2 (color online). Diagrammatic representation of the gluon mass equation.

both of its sides to be written in terms of the RGI quantities introduced in the previous section.

As was demonstrated in Ref. [21], the complete gluon mass equation is given by (see Fig. 2)

$$m^2(q^2) = \frac{1}{2}\frac{ig^2 C_A}{1+G(q^2)}\frac{q_\mu q_\nu}{q^2}\int_k [(a_0)+2(a_5)]^{\mu\alpha\beta}\Delta_{\alpha\rho}(k) \times \Delta_{\beta\sigma}(k+q)\tilde{V}^{\nu\rho\sigma}(q,k,-k-q), \tag{3.1}$$

where C_A is the Casimir eigenvalue in the adjoint representation [$C_A = N$ for $SU(N)$]; $\tilde{V}$ is the pole vertex introduced in the previous section; (a_0) is simply the tree-level three-gluon vertex,

$$(a_0)_{\mu\alpha\beta} = \Gamma^{(0)}_{\mu\alpha\beta}(q,k,-k-q), \tag{3.2}$$

with

$$\Gamma^{(0)}_{\mu\alpha\beta}(q,r,p) = (q-r)_\beta g_{\alpha\mu} + (r-p)_\mu g_{\alpha\beta} + (p-q)_\alpha g_{\mu\beta}; \tag{3.3}$$

and (a_5) denotes the vertex subgraph nested in the "two-loop" self-energy graph (see also Fig. 3).

Using the fact that $\tilde{V}$ satisfies the WI of Eq. (2.21), i.e.,

$$q^\nu \tilde{V}_{\nu\rho\sigma}(q,k,-k-q) = m^2(k)P_{\rho\sigma}(k) - m^2(k+q)P_{\rho\sigma}(k+q), \tag{3.4}$$

and after appropriate shifts of the integration variable, we arrive at [21]

$$m^2(q^2) = \frac{ig^2 C_A}{1+G(q^2)}\frac{q_\mu}{q^2}\int_k [(a_0)+(a_4) + (a_5)]^{\mu\alpha\beta}\Delta_{\alpha\rho}(k)\Delta^\rho_\beta(k+q)m^2(k^2), \tag{3.5}$$

where $(a_4)_{\mu\alpha\beta}(q,r,p) = -(a_5)_{\mu\beta\alpha}(q,p,r)$ (see also the first row of Fig. 3).

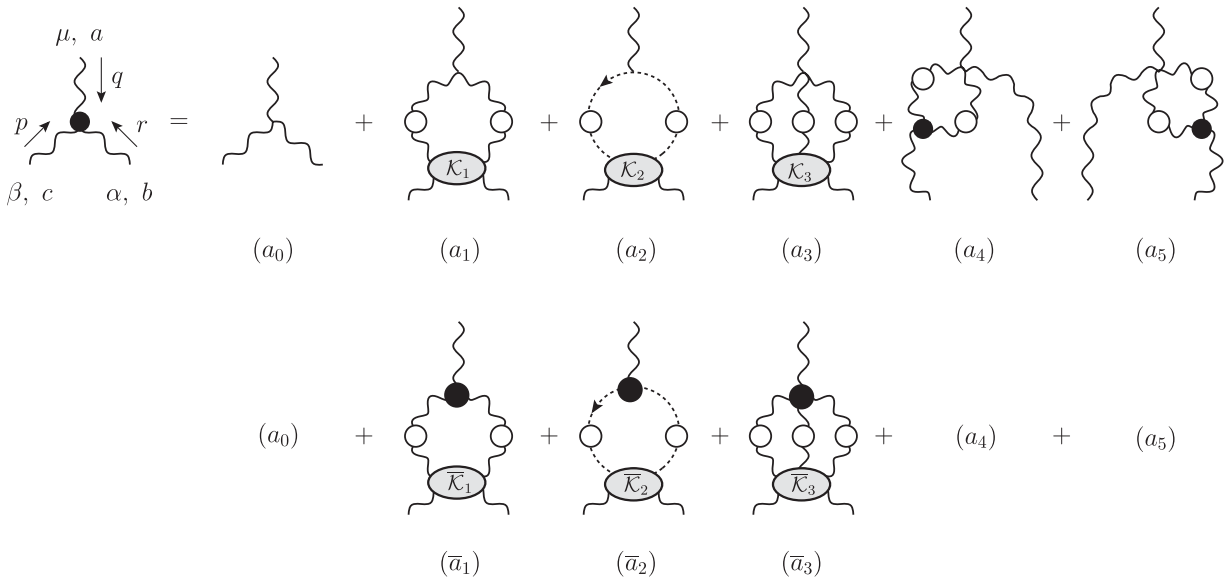

FIG. 3. The SDE for the three gluon vertex, in the conventional (first row) and Bethe–Salpeter version (second row). Note that the Bose symmetry of $\Gamma^{abc}_{\mu\alpha\beta}(q,r,p)$ implies that $(a_4)^{abc}_{\mu\alpha\beta}(q,r,p) = (a_5)^{acb}_{\mu\beta\alpha}(q,p,r)$; when the color has been factored out, as in Eq. (3.5), we have instead $(a_4)_{\mu\alpha\beta}(q,r,p) = -(a_5)_{\mu\beta\alpha}(q,p,r)$.

Let us now turn to the SDE satisfied by the conventional (Q^3) three-gluon vertex $\Gamma^{abc}_{\mu\alpha\beta}(q,r,p)$, shown diagrammatically in Fig. 3, and derive a relation necessary for the treatment of Eq. (3.5). On the first line of Fig. 3, the vertex SDE is expressed in terms of the standard multiparticle kernels, $\mathcal{K}_i$, while on the second the Bethe–Salpeter version of the same equation is presented. Note that in this latter version the vertices with the external momentum q are fully dressed; consequently, the corresponding Bethe–Salpeter kernels, $\bar{\mathcal{K}}_i$, differ from the $\mathcal{K}_i$, since certain diagrams, allotted to dress the vertices, must be excluded from them, in order to avoid overcounting ($\bar{\mathcal{K}}_i$ and $\mathcal{K}_i$ are related through a nonlinear integral equation—see, e.g., Refs. [1] and [39]).

If we express the various diagrams (a_i) in terms of renormalized quantities, denoting by (a_i^R) the resulting expressions, it is relatively straightforward to demonstrate that

$$(\bar{a}_1) = Z_3^{-1}(\bar{a}_1^R); \quad (\bar{a}_2) = Z_3^{-1}(\bar{a}_2^R); \quad (\bar{a}_3) = Z_3^{-1}(\bar{a}_3^R);$$
$$(a_4) = Z_g^2 Z_A^2 Z_3^{-1}(a_4^R); \quad (a_5) = Z_g^2 Z_A^2 Z_3^{-1}(a_5^R). \tag{3.6}$$

Thus, for the original, unrenormalized vertex SDE, we have (suppressing all indices)

$$\begin{aligned}\Gamma &= (a_0) + (a_4) + (a_5) + (\bar{a}_1) + (\bar{a}_2) + (\bar{a}_3) \\ &= (a_0) + Z_g^2 Z_A^2 Z_3^{-1}[(a_4^R) + (a_5^R)] \\ &\quad + Z_3^{-1}[(\bar{a}_1^R) + (\bar{a}_2^R) + (\bar{a}_3^R)],\end{aligned} \tag{3.7}$$

and so, after introducing the renormalized vertex $\Gamma_R = Z_3\Gamma$ [see Eq. (2.9)], we arrive at

$$Z_3(a_0) + Z_g^2 Z_A^2[(a_4^R) + (a_5^R)] = \Gamma_R - [(\bar{a}_1^R) + (\bar{a}_2^R) + (\bar{a}_3^R)]. \tag{3.8}$$

Returning to Eq. (3.5), and rewriting it in terms of renormalized quantities, we have

$$m_R^2(q^2) = \frac{iC_A g_R^2}{1+G_R(q^2)}\frac{q_\mu}{q^2}\int_k \{Z_3(a_0) + Z_g^2 Z_A^2[(a_4^R) + (a_5^R)]\}^{\mu\alpha\beta}\Delta_{\alpha\rho}^R(k)\Delta_\beta^{R\rho}(k+q)m_R^2(k^2), \tag{3.9}$$

which, in view of Eq. (3.8), may be written exclusively in terms of renormalized quantities (i.e., with no reference to the cutoff-dependent Z_i), as

$$m_R^2(q^2) = \frac{iC_A g_R^2}{1+G_R(q^2)}\frac{q_\mu}{q^2}\int_k \mathcal{G}^{\mu\alpha\beta}\Delta_{\alpha\rho}^R(k)\Delta_\beta^{R\rho}(k+q)m_R^2(k^2), \tag{3.10}$$

where

$$\mathcal{G}^{\mu\alpha\beta} \equiv \left[\Gamma_R - \sum_{i=1}^{3}(\bar{a}_i^R)\right]^{\mu\alpha\beta}, \tag{3.11}$$

namely, the rhs of Eq. (3.8).

We next study the properties of Eq. (3.10) under RG transformations. To that end, it is convenient to recast both sides of this equation in terms of appropriately chosen RGI quantities. Clearly, by virtue of Eq. (2.30), a simple multiplication by $g^{-2}[1+G(q^2)]^2$ converts the lhs of Eq. (3.10) into the RGI mass $\bar{m}^2(q^2)$ introduced in Eq. (2.30). On the other hand, the demonstration that, after the aforementioned multiplication, the rhs is also RGI is slightly more involved.

To prove this statement, we will employ the three RGI quantities, $\mathcal{R}_i$, introduced in Eq. (2.31). In particular, it is relatively straightforward to establish that when the terms $(\bar{a}_i^R)$ are multiplied by the factor $g_R\Delta_R^{1/2}(q)\Delta_R^{1/2}(r)\Delta_R^{1/2}(p)$ they become functions of the $\mathcal{R}_i$; so, we have (see Fig. 4)

$$g_R\Delta_R^{1/2}(q)\Delta_R^{1/2}(r)\Delta_R^{1/2}(p)(\bar{a}_i^R) = \mathcal{F}_i(\mathcal{R}_1,\mathcal{R}_2,\mathcal{R}_3). \tag{3.12}$$

As a consequence,

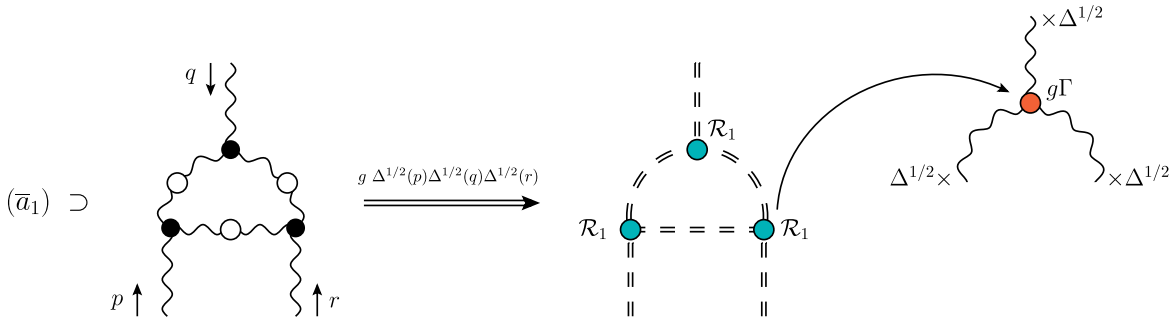

FIG. 4 (color online). Schematic representation of the conversion of a typical diagram into its RGI equivalent.

$$g_R \Delta_R^{1/2}(q)\Delta_R^{1/2}(r)\Delta_R^{1/2}(p)\mathcal{G}(q,r,p) = \mathcal{R}_1 - \sum_{i=1}^{3}\mathcal{F}_i \equiv \mathcal{R}. \tag{3.13}$$

Note finally that the ratio $f(p_1)/f(p_2)$ of any two-point function $f(p)$ is also a RGI quantity.

Armed with these results, we may now reexpress Eq. (3.10) in terms of manifestly RGI quantities. Specifically, after the aforementioned multiplication by $g^{-2}[1+G(q^2)]^2$, and some appropriate manipulations, we arrive at [with $p=-(k+q)$]

$$\bar{m}^2(q^2) = \frac{iC_A q_\mu}{q^2 d^{1/2}(q^2)}\int_k \mathcal{R}^{\mu\alpha\beta}P_{\alpha\rho}(k)P^{\rho}_{\beta}(p)d^{1/2}(k^2)d^{1/2}(p^2) \times\left\{\frac{1+G(p^2)}{1+G(k^2)}\right\}\bar{m}^2(k^2), \tag{3.14}$$

which is a manifestly RGI integral equation.

IV. GENERAL STRUCTURE OF THE THREE-GLUON KERNEL

In the previous section, we demonstrated that the mass equation, as captured in Eq. (3.10), has built in it the exact RG properties that one expects on general theoretical grounds. Evidently, in order to proceed further, and deduce from Eq. (3.10) the momentum dependence of the gluon mass, further information on $\mathcal{G}^{\mu\alpha\beta}$, or directly on its divergence, $q_\mu\mathcal{G}^{\mu\alpha\beta}$, is needed.

It is clear that the diagrammatic decomposition of $\mathcal{G}^{\mu\alpha\beta}$ involves the three Bethe–Salpeter kernels $\bar{K}_1$, $\bar{K}_2$, and $\bar{K}_3$, for which the complicated skeleton expansion renders their full determination impossible. It is therefore necessary, for practical purposes, to introduce approximations or Ansätze for the quantity $\mathcal{G}^{\mu\alpha\beta}$, which ought to encode, as well as possible, some of its salient field-theoretic properties.

To that end, it is essential to consider the tensorial decomposition of $\mathcal{G}^{\mu\alpha\beta}$ and exploit its Bose-symmetric nature, together with the fact that, when inserted into Eq. (3.10), it is contracted by two transverse projectors. Specifically, in a straightforward basis composed by the momenta r and p, one has[1]

$$\mathcal{G}^{\mu\alpha\beta}(q,r,p) = \sum_{i=1}^{14} C_i(q,r,p)b_i^{\mu\alpha\beta}, \tag{4.1}$$

with

$$b_1^{\mu\alpha\beta} = r^\mu g^{\alpha\beta}; \quad b_2^{\mu\alpha\beta} = p^\mu g^{\alpha\beta}; \quad b_3^{\mu\alpha\beta} = p^\alpha g^{\mu\beta};$$
$$b_4^{\mu\alpha\beta} = r^\beta g^{\mu\alpha}; \quad b_5^{\mu\alpha\beta} = p^\mu p^\alpha r^\beta; \quad b_6^{\mu\alpha\beta} = r^\mu p^\alpha r^\beta \tag{4.2}$$

[1]Alternatively, one may use the standard Ball and Chiu decomposition [69], arriving at exactly the same conclusions.

and

$$b_7^{\mu\alpha\beta} = p^\beta g^{\mu\alpha}; \quad b_8^{\mu\alpha\beta} = r^\alpha g^{\mu\beta}; \quad b_9^{\mu\alpha\beta} = r^\mu r^\alpha r^\beta;$$
$$b_{10}^{\mu\alpha\beta} = p^\mu p^\alpha p^\beta; \quad b_{11}^{\mu\alpha\beta} = p^\mu r^\alpha p^\beta; \quad b_{12}^{\mu\alpha\beta} = p^\mu r^\alpha r^\beta;$$
$$b_{13}^{\mu\alpha\beta} = r^\mu p^\alpha p^\beta; \quad b_{14}^{\mu\alpha\beta} = r^\mu p^\alpha p^\beta. \tag{4.3}$$

The form factors $C_i(q,r,p)$ are in general related among each other by conditions imposed by Bose symmetry. Particularly important to our purposes are the relations

$$C_2(q,r,p) = -C_1(q,p,r);$$
$$C_4(q,r,p) = -C_3(q,p,r). \tag{4.4}$$

The tree-level values of the form factors C_i are determined by setting $\mathcal{G}=\Gamma^{(0)}$; as one can check by substituting $q=-(r+p)$ into Eq. (3.2), and using the above basis to express the result, one has $C_1^{(0)}=1$, $C_2^{(0)}=-1$, $C_3^{(0)}=2$, $C_4^{(0)}=-2$, $C_7^{(0)}=-1$, $C_8^{(0)}=1$, with all the remaining Cs vanishing.

Now, when contracted with $P_{\alpha\rho}(r)P^{\rho}_{\beta}(p)$, the second set of tensors, $(b_7)-(b_{14})$, vanishes identically, while for the first set, one can effectively use the replacements

$$b_3^{\mu\alpha\beta} \to -q^\alpha g^{\mu\beta}; \quad b_4^{\mu\alpha\beta} \to -q^\beta g^{\mu\alpha};$$
$$b_5^{\mu\alpha\beta} \to p^\mu q^\alpha q^\beta; \quad b_6^{\mu\alpha\beta} \to r^\mu q^\alpha q^\beta. \tag{4.5}$$

It is then relatively straightforward to establish that

$$q_\mu\mathcal{G}^{\mu\alpha\beta}P_{\alpha\rho}(r)P^{\rho}_{\beta}(p) = \{[(p^2-r^2)S + q^2A]g^{\alpha\beta} + Bq^\alpha q^\beta\} \times P_{\alpha\rho}(r)P^{\rho}_{\beta}(p), \tag{4.6}$$

where

$$S(q,r,p) = \frac{1}{2}[C_1(q,r,p)+C_1(q,p,r)],$$
$$A(q,r,p) = \frac{1}{2}[C_1(q,p,r)-C_1(q,r,p)],$$
$$B(q,r,p) = (q\cdot p)C_5(q,r,p) + (q\cdot r)C_6(q,r,p) + [C_3(q,p,r)-C_3(q,r,p)]. \tag{4.7}$$

The terms A and B emerge when writing the total contribution from b_1 and b_2 as the sum of a symmetric piece and an antisymmetric piece under $r\leftrightarrow p$, namely,

$$[C_1(q,r,p)r^\mu + C_2(q,r,p)p^\mu]g^{\alpha\beta} = [S(q,r,p)(r-p)^\mu + A(q,r,p)q^\mu]g^{\alpha\beta}. \tag{4.8}$$

In addition, note that we have used Eq. (4.4) to eliminate C_2 and C_4 in favor of C_1 and C_3, respectively.

Let us now comment on the way that the terms of Eq. (4.7) contribute to the mass equation in the limit $q\to 0$.

It is easy to verify that the terms associated with $A(q,r,p)$ and $B(q,r,p)$ are subleading in this limit. Indeed, first of all, the q^2 that multiplies the $A(q,r,p)$ and the $q^\alpha q^\beta$ that multiplies $B(q,r,p)$ compensate the $(1/q^2)$ in front of the mass equation. Then, since $A(q,r,p)$ is antisymmetric under $r\leftrightarrow p$, we have that $A(0,-p,p)=0$, and therefore, when $q\to 0$, $A(q,r,p)\to\mathcal{O}(q)$. Similarly, the terms in B proportional to C_5 and C_6 are multiplied by an additional power of q and are manifestly subleading, while the remaining term is antisymmetric under $r\leftrightarrow p$, and therefore this, too, is of order $\mathcal{O}(q)$. Thus, the only term that contributes to the mass equation in the IR limit is the one associated with S. Note finally that out of the three terms defined in Eq. (4.7), only S has a tree-level value, namely, $S^{(0)}=1$.

After these considerations, we can write down the final form taken by the mass equation. Setting $r=k$, $p=-(k+q)$, and passing to Euclidean space following standard rules [21] (and suppressing the index "E" throughout), we have

$$m^2(q^2)=-\frac{g^2C_A}{1+G(q^2)}\frac{1}{q^2}\int_k m^2(k^2)\Delta_{\alpha\rho}(k)\Delta^\rho_\beta(k+q)\times\mathcal{K}^{\alpha\beta}(q,k,-k-q),\tag{4.9}$$

where, according to the above discussion, the total kernel $\mathcal{K}^{\alpha\beta}$ may be naturally decomposed into a contribution that is leading in the IR, to be denoted by $\mathcal{K}^{\alpha\beta}_{\rm L}$, and one that is subleading, to be denoted by $\mathcal{K}^{\alpha\beta}_{\rm SL}$, namely,

$$\mathcal{K}^{\alpha\beta}=\mathcal{K}^{\alpha\beta}_{\rm L}+\mathcal{K}^{\alpha\beta}_{\rm SL},\tag{4.10}$$

with

$$\mathcal{K}^{\alpha\beta}_{\rm L}=[(k+q)^2-k^2]Sg^{\alpha\beta},\qquad \mathcal{K}^{\alpha\beta}_{\rm SL}=q^2Ag^{\alpha\beta}+Bq^\alpha q^\beta,\tag{4.11}$$

where the common argument $(q,k,-q-k)$ in all above quantities has been suppressed.

V. RG PROPERTIES OF THE ORIGINAL MASS EQUATION

Let us now compare Eq. (4.9) with the one derived originally in Ref. [21]. There, the mass equation considered had the form of Eq. (3.9); in other words, one dealt directly with the term $[Z_3(a_0)+Z_g^2Z_A^2[(a_4^R)+(a_5^R)]$, without passing to the rhs of Eq. (3.8). The way to handle the renormalization constants was to set them directly equal to unity and *assume* that the remaining terms had been rendered UV finite. This procedure finally amounted to the effective replacement

$$q_\mu\{Z_3(a_0)+Z_g^2Z_A^2[(a_4^R)+(a_5^R)]\}^{\mu\alpha\beta}\to\mathcal{K}^{\alpha\beta}(k,q),\tag{5.1}$$

with

$$\mathcal{K}^{\alpha\beta}(k,q)=[(k+q)^2-k^2]\{1-[Y_R(k+q)+Y_R(k)]\}g^{\alpha\beta}+[Y_R(k+q)-Y_R(k)](q^2g^{\alpha\beta}-2q^\alpha q^\beta),\tag{5.2}$$

where

$$Y(k^2)=\frac{g^2C_A}{4k^2}k_\alpha\int_\ell\Delta^{\alpha\rho}(\ell)\Delta^{\beta\sigma}(\ell+k)\Gamma_{\sigma\rho\beta}(-\ell-k,\ell,k).\tag{5.3}$$

The renormalized version of Y is simply

$$Y_R(k)=Y(k)-Y(\mu),\tag{5.4}$$

namely, the form corresponding to the momentum-subtraction (MOM) scheme.

A direct comparison of Eq. (5.2) with the generic form given in Eq. (4.11) establishes that, in this case,

$$S=1-[Y_R(k+q)+Y_R(k)];\qquad A=Y_R(k+q)-Y_R(k);\qquad B=-2A.\tag{5.5}$$

Note that S is symmetric under the interchange $k\leftrightarrow(k+q)$, as expected from its general property given in Eq. (4.7); similarly, the A of Eq. (5.5) is antisymmetric under the same interchange, exactly as the A of Eq. (4.7). Finally, $S^{(0)}=1$, as it should.

In Ref. [21] an approximate form for $Y(k)$ was obtained by substituting tree-level expressions for all quantities appearing inside the integral in Eq. (5.3). The result is given by

$$Y_R(k^2)=-\frac{15}{16}t(k),\tag{5.6}$$

where

$$t(k)\equiv\left(\frac{\alpha_sC_A}{4\pi}\right)\log\left(\frac{k^2}{\mu^2}\right),\tag{5.7}$$

and $\alpha_s=g^2/4\pi$ is the value of the Yang–Mills charge at the subtraction point μ chosen.

In the analysis of the gluon mass equation presented in Ref. [21], the rhs of Eq. (5.6) was multiplied by a constant C, with $C>1$. As has been explained in detail there, the main reason for this is the need to counteract the (destabilizing) effect of the negative sign in front of the integral on the rhs of Eq. (4.9) and obtain positive-definite solutions for the gluon mass, at least within a reasonable range of physical momenta. In particular, for $\alpha_s=0.22$, which is the "canonical" MOM value for $\mu=4.3$ GeV, and $C=9.2$, the function $m^2(q^2)$ is positive in the range of momenta between 0 to 5.5 GeV; past that point it turns negative (but its magnitude is extremely small, around 10^{-5}GeV^2, as

shown in the inset of Fig. 10) [70]. As we will see in the next section, this unwanted feature may be eventually rectified by modifying appropriately the form of S.

A. Quantifying the kernel quality: Basic procedure

To quantitatively determine to what extent a given approximation for S respects the RG properties of the full mass equation, it is necessary to establish a reference situation and then compute possible deviations from it. To that end, we will employ a general procedure that consists of the following main steps:

(i) We consider the RGI quantity

$$d(q^2) = g^2 F^2(q^2)\Delta(q^2), \tag{5.8}$$

namely, that of Eq. (2.29) with the approximation Eq. (2.5) implemented and compute its shape using $F(q^2)$ and $\Delta(q^2)$ from the lattice, for different values of the renormalization point μ. To that end, we use the standard formulas [27]

$$\Delta(q^2,\mu^2) = \frac{\Delta(q^2,\nu^2)}{\mu^2\Delta(\mu^2,\nu^2)}, \qquad F(q^2,\mu^2) = \frac{F(q^2,\nu^2)}{F(\mu^2,\nu^2)}, \tag{5.9}$$

which allow one to connect a set of lattice data renormalized at μ with the corresponding set renormalized at ν. It is clear that, since these changes amount to the multiplication of the product $F^2(q^2)\Delta(q^2)$ by an overall constant, we can adjust the value of g^2 (or α_s) for each μ, such that the curves of $d(q^2)$ so produced lie exactly on top of each other. Thus, this procedure fixes the values of $\alpha_s(\mu)$, such that the (formally RGI) $d(q^2)$ is indeed RGI. As we will see, the resulting values for $\alpha_s(\mu)$ are rather compatible with those predicted by standard MOM calculations.

(ii) We next solve the gluon mass equation for the same set of μ's used in the previous step. Specifically, for the ingredients entering in the rhs of Eq. (4.9), such as g^2, F, and Δ, we use the corresponding quantities found in (i), for any given μ; note that Y_R is also μ dependent and is accordingly modified. This procedure furnishes a set of μ-dependent solutions, $m^2(q^2,\mu^2)$; note that the value of the constant C that multiplies Y_R also varies (rather mildly) with μ.

(iii) The various masses, $m^2(q^2,\mu^2)$, found in (ii) are now used to construct the RGI mass defined in Eq. (2.30) [using again Eq. (2.5)], namely,

$$\bar{m}^2(q^2) = \frac{m^2(q^2)}{g^2F^2(q^2)}. \tag{5.10}$$

Now, ideally speaking, when the various $m^2(q^2,\mu^2)$ are inserted into Eq. (5.10), together with the corresponding (μ-dependent) $g^2F^2(q^2)$, one ought to obtain the same identical curve for each value of μ.

In practice, of course, deviations between the various curves are expected, precisely because our knowledge of S is imperfect. Therefore, a theoretically motivated way to discriminate between possible approximation for S is to choose the one that produces the best coincidence (in the sense of minimizing the relative error) for the various $\bar{m}^2(q^2)$.

B. Numerical analysis

Throughout the numerical study presented here, as well as in the next section, we will evaluate the relevant field-theoretic quantities at three different values of the renormalization point μ_i; in particular, we will use $\mu_1 = 4.3$ GeV, $\mu_2 = 3.0$ GeV, and $\mu_3 = 2.5$ GeV. In the various plots, the curves of a quantity $A(q^2,\mu_i^2)$ produced for these three different values of μ_i will be depicted as follows: $A(q^2,\mu_1^2)$ with squares or solid (black) curve, $A(q^2,\mu_2^2)$ with circles or dotted (red) curve, and $A(q^2,\mu_3^2)$ with triangles or dashed (blue) curve.

The first step in this analysis is to consider the lattice data for $\Delta(q^2)$ and $F(q^2)$ given in Ref. [30]; these data are fitted using the functional forms reported in various recent articles [20,37,71]. Then, repeated use of Eq. (5.9) allows us to generate the three curves for $\Delta(q^2)$ and $F(q^2)$ renormalized at μ_i (with $i = 1, 2, 3$), which are shown in Fig. 5. It is clear that, due to multiplicative renormalizability, expressed by Eq. (5.9), each curve may be obtained from the other by a simple rescaling. Specifically, the curves $\Delta(q^2,\mu_2^2)$ and $\Delta(q^2,\mu_3^2)$ are obtained from $\Delta(q^2,\mu_1^2)$ through multiplication by the factors of 1.20 and 1.33, respectively; in the case of $F(q^2)$, the corresponding rescaling factors are 1.09 and 1.15.

Next, we form the RGI combination $d(q^2)$ given in Eq. (5.8). Concretely, for each specific value of μ_i, we combine the corresponding ingredients entering into the definition of $d(q^2)$. As mentioned before in step (i), the value of g^2 (or α_s) for each μ_i is fixed by requiring that the three curves of $d(q^2)$ so produced lie exactly on top of each other; so, the corresponding $\alpha_s(\mu_i)$ must be rescaled by an amount that will exactly compensate the corresponding rescalings introduced to the product $\Delta(q^2,\mu_i^2)F^2(q^2,\mu_i^2)$. Specifically, starting with $\alpha_s(\mu_1^2) = 0.220$, which is the value that best fits the lattice data in the recent SDE analysis presented in Ref. [72], we obtain the values $\alpha_s(\mu_2^2) = 0.320$ and $\alpha_s(\mu_3^2) = 0.392$.

On the left panel of Fig. 6, we plot the three curves for the dimensionful quantity $d(q^2)/4\pi$. As expected, by construction, we can see that the three curves are indeed on top of each other, thus making manifest that, for the particular set of values of $\alpha_s(\mu_i)$ quoted above, $d(q^2)$ is μ independent.

It is important at this point to check whether the values for $\alpha_s(\mu_i)$ obtained from the above procedure are

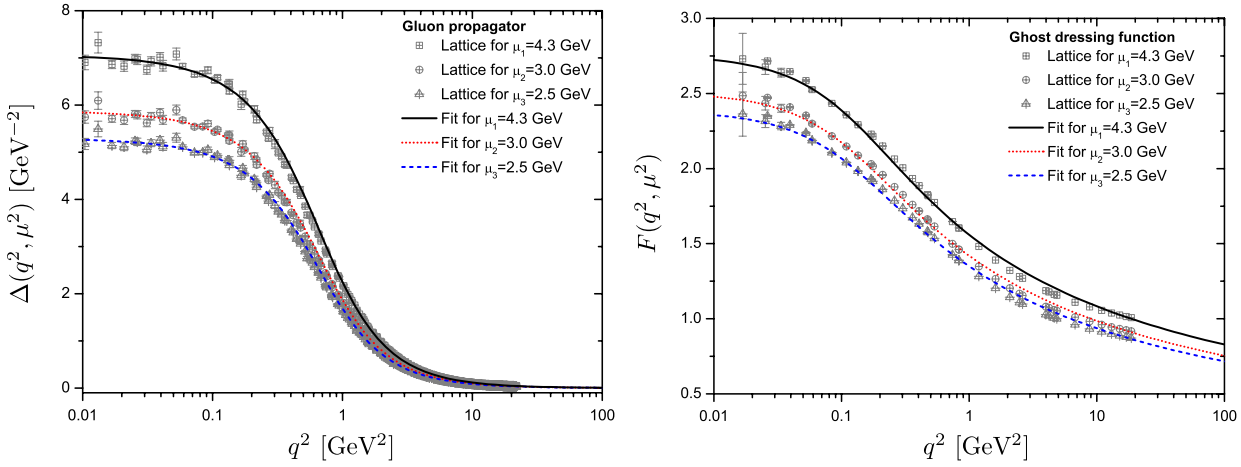

FIG. 5 (color online). The quenched lattice data and the corresponding fits for the $SU(3)$ gluon propagator (left panel) and ghost dressing function (right panel) renormalized at three different scales μ_i. Lattice data are taken from Ref. [30].

compatible with the MOM expectations. This is done in the right panel of the same figure, where the gray continuous line represents the $\alpha_{\rm MOM}(q^2)$ obtained from the nonperturbative analysis of Ref. [73], for $\Lambda_{\rm QCD} = 350$ MeV and $N_f = 0$; the aforementioned three values used for $\alpha_s(\mu_i)$ are denoted by the corresponding symbols. As we can see, the values of $\alpha_s(\mu_i)$ that implement the μ independence of $d(q^2)$ are indeed in good agreement with the MOM predictions.

We now turn to the gluon mass equation; evidently, since its kernel is composed of μ-dependent quantities, for each value of μ_i, we will obtain a different solution, $m^2(q^2,\mu_i^2)$. On the left panel of Fig. 7, we show the corresponding solutions for the three renormalization points chosen. The corresponding infrared saturation points, $m^2(0,\mu_i^2) = \Delta^{-1}(0,\mu_i^2)$, are given by $m(0,\mu_1^2) = 375\,\text{MeV}$, $m(0,\mu_2^2) = 412$ MeV, and $m(0,\mu_3^2) = 434$ MeV. In addition, as anticipated, also the values of the arbitrary constant C display a mild μ dependence: $C(\mu_1) = 9.2$, $C(\mu_2) = 8.5$, and $C(\mu_3) = 8.4$.

Now we are in the position to determine the behavior of the RGI mass $\bar{m}^2(q^2)$. To that end, we substitute into Eq. (5.10) the μ-dependent results for $m^2(q^2,\mu_i^2)$, $F(q^2,\mu_i^2)$, and $\alpha_s(\mu_i)$ obtained above. This is shown on the right panel of Fig. 7, where we plot the quantity $4\pi\bar{m}^2(q^2)$ for the three values of μ_i. As we can see, we have a nice agreement between the three curves in the range from 0 to 0.05 GeV^2. However, for higher values of q^2, they separate from the other, reaching the biggest discrepancy at $q^2 = 7.5$ GeV^2, where the percentage error between the (black) continuous and the (blue) dashed curves is around 64%.

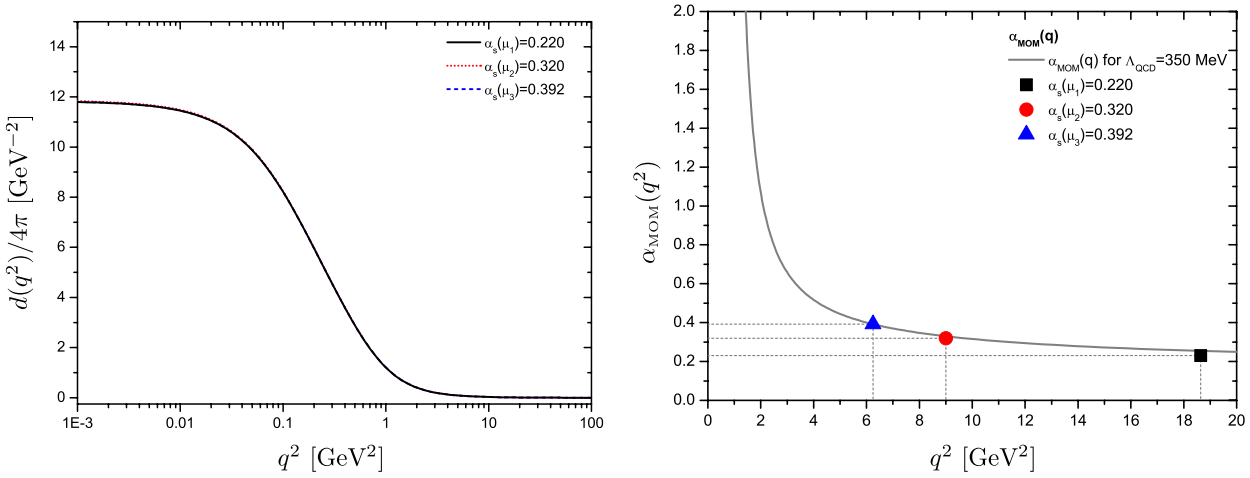

FIG. 6 (color online). Left panel: The RGI combination $d(q^2)/4\pi$ obtained using Eq. (2.29) for the three renormalization points μ_i chosen. Right panel: The running coupling in the MOM scheme, $\alpha_{\rm MOM}(q)$ [73] for $\Lambda_{\rm QCD} = 350$ GeV and $N_f = 0$. Each point represents the values used for $\alpha_s(\mu_i)$ in our calculations.

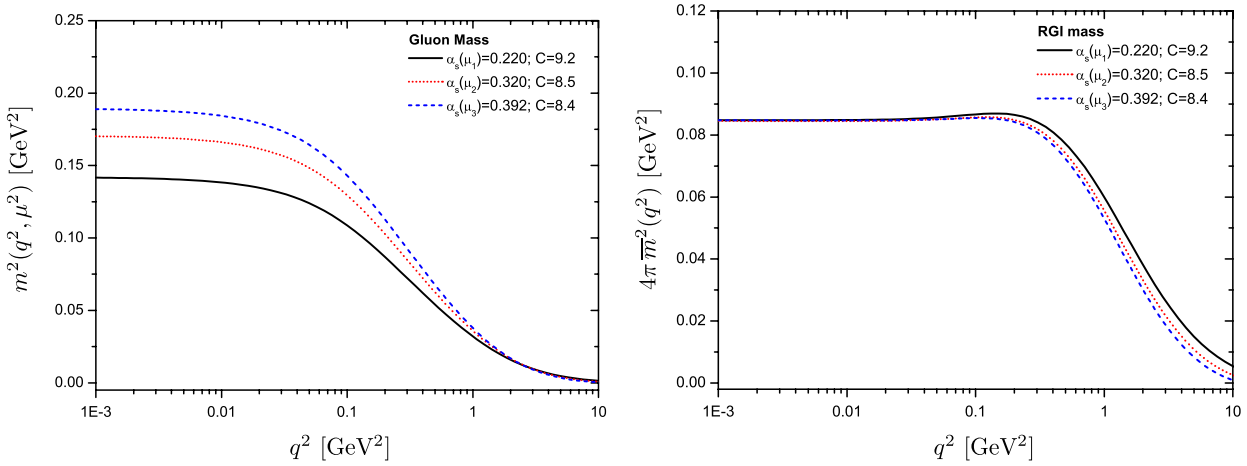

FIG. 7 (color online). Left panel: The numerical solution for the dynamical gluon mass, $m^2(q^2,\mu^2)$, for the three values of μ_i. Right panel: The corresponding RGI mass $4\pi\bar{m}^2(q^2)$ obtained from Eq. (2.30) for the three values of μ_i.

Evidently, the considerable deviations from the exact RG invariance displayed in Fig. 7 indicate that the form of the function S employed in the mass equation needs to be improved. As we will see in the next section with some specific examples, such an improvement is indeed possible and can be obtained by resorting to basic RGI arguments.

VI. RG IMPROVED VERSIONS OF THE KERNEL

As has been established in Eq. (3.13), the quantity $\mathcal{G}$ must be such that, when multiplied by $g\Delta^{1/2}(q)\Delta^{1/2}(r)\Delta^{1/2}(p)$, it ought to give rise to an RGI combination. This information may be used to obtain some well-motivated Ansätze for S, which, in turn, may lead to solutions for $m^2(q^2)$ that are more well behaved under the RG. In this section we will explore the explicit realization of this possibility. The study presented here is by no means exhaustive; it is simply indicative of how RG-improved versions of the gluon mass equation may be obtained in principle.

A. Two simple models

Specifically, let us set

$$S(q,k,k+q) = F(q)W(k,k+q), \tag{6.1}$$

where, in accordance with the general properties of S, the W is symmetric under the exchange $k\leftrightarrow k+q$. In addition, at tree level we must have $W^{(0)}=1$, so that, since $F^{(0)}(q)=1$, we get $S^{(0)}=1$, as required.

If we now use the S of Eq. (6.1) to construct the lhs of Eq. (3.13), we have

$$\begin{aligned} &g\Delta^{1/2}(q)\Delta^{1/2}(k)\Delta^{1/2}(k+q)S \\ &\quad = [gF(q)\Delta^{1/2}(q)]\{\Delta^{1/2}(k)\Delta^{1/2}(k+q)W(k,k+q)\} \\ &\quad = d^{1/2}(q^2)\{\Delta^{1/2}(k)\Delta^{1/2}(k+q)W(k,k+q)\}. \end{aligned} \tag{6.2}$$

It is clear now that the presence of $F(q)$ facilitates the realization of the RGI combination, by providing the missing ingredient for the formation of $d^{1/2}(q^2)$; it is, therefore, an advantageous starting point. The remaining structure must obviously come from W, which must convert the combination inside the curly bracket into another RGI quantity.

In order to devise an approximate expression for the (dimensionless) W, let us first consider the one-loop expression of $\Delta^{-1}(k)=k^2J(k)$, in the MOM scheme. For the (dimensionless) $J(k^2)$, we have

$$J(k) = 1+\frac{13}{6}t(k), \tag{6.3}$$

and so

$$J^{1/2}(k)J^{1/2}(k+q) = 1+\frac{13}{12}[t(k)+t(k+q)]+\mathcal{O}(\alpha_s^2). \tag{6.4}$$

Thus, at order $\mathcal{O}(\alpha_s)$ the minimal necessary structure for W is

$$W^{(1)} = 1+\frac{13}{12}[t(k)+t(k+q)]. \tag{6.5}$$

Of course, this minimal form may be multiplied by a μ-independent function, which, at the given order, will provide the (unknown) rhs of Eq. (3.13). Evidently, use of the minimal $W^{(1)}$ gives rise to a lhs equal to unity.

These observations motivate the study of two simple extensions of Eq. (6.5), where some additional structure has been added in order to model higher-order effects or purely nonperturbative contributions.

The cases we will consider are

$$\begin{aligned} W_1 = 1+\frac{13}{12}[t(k)+t(k+q)]+c_1[t^2(k)+t^2(k+q)] \\ +c_2t(k)t(k+q) \end{aligned} \tag{6.6}$$

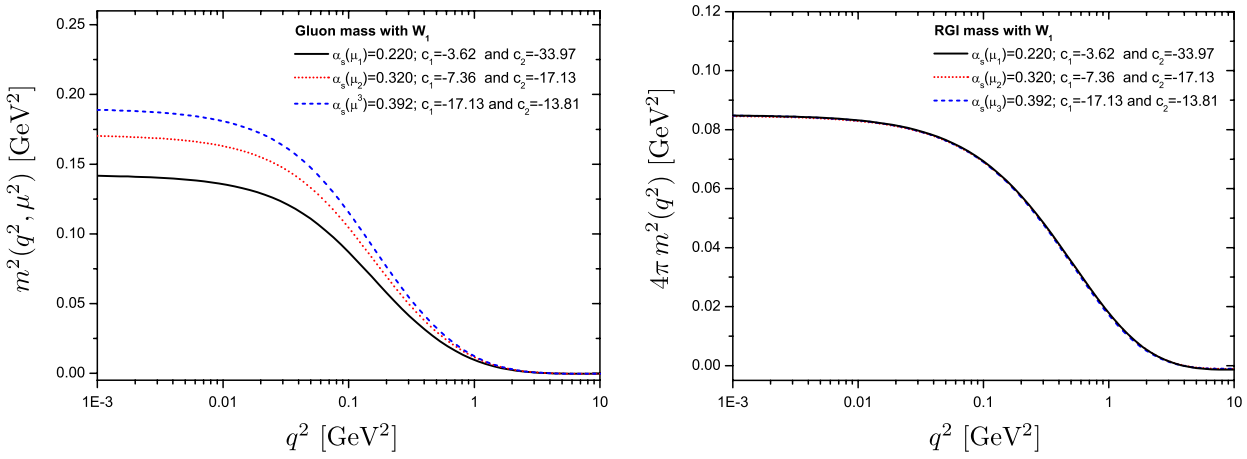

FIG. 8 (color online). The gluon dynamical mass $m^2(q^2,\mu^2)$ (left panel) and the corresponding RGI mass $4\pi\bar{m}^2(q^2)$ (right panel) obtained using the model of Eq. (6.6) for the three values of μ_i.

and

$$W_2 = 1 + \frac{13}{12}[t(k) + t(k+q)] + c. \tag{6.7}$$

We next study the numerical implications of the above two possibilities.

B. Numerical analysis

On the left panel of Fig. 8, we show the numerical solution for $m^2(q^2,\mu_i^2)$ using the model presented in Eq. (6.6). In particular, we choose, for the three different μ_i, the parameters $c_1(\mu_1) = -3.62$ and $c_2(\mu_1) = -33.97$; $c_1(\mu_2) = -7.36$ and $c_2(\mu_2) = -17.13$; and $c_1(\mu_3) = -7.42$ and $c_2(\mu_3) = -13.81$.

Although the general qualitative behavior of $m^2(q^2)$ appears rather similar to that shown in Fig. 7, the RGI masses obtained from them show a definite improvement with respect to those of Fig. 7. Indeed, as one can clearly see on the right panel of Fig. 8, the three curves coincide within a wider range of momenta than in the previous case. More specifically, the less favorable region of momenta is around $q^2 \approx 3.5$ GeV^2, where the relative error between the curves is smaller than 12%. However, the downside of the form W_1 is that the appearance of a negative UV tail for $m^2(q^2)$ (past $q^2 \approx 3.5$ GeV^2) persists.

It is important to mention that the mass equation admits solutions for a variety of additional choices for $c_1(\mu_i)$ and $c_2(\mu_i)$; however, the particular values quoted above are singled out because they yield $\bar{m}^2(q^2)$ that are as close to being perfectly RGI as possible. In that sense, our scanning through the possible values of $c_1(\mu_i)$ and $c_2(\mu_i)$ is by no means exhaustive, but only indicative of certain general trends in the type of solutions obtained.

We next analyze the second model, where Eq. (6.7) is used in the kernel of the gluon mass equation. The results for this particular case are presented in Fig. 9. On the left panel, we plot $m^2(q^2,\mu_i^2)$ for the three values of μ_i chosen. The right panel shows the RGI quantity $4\pi\bar{m}^2(q^2)$; evidently, the results for the three μ_i practically collapse on a

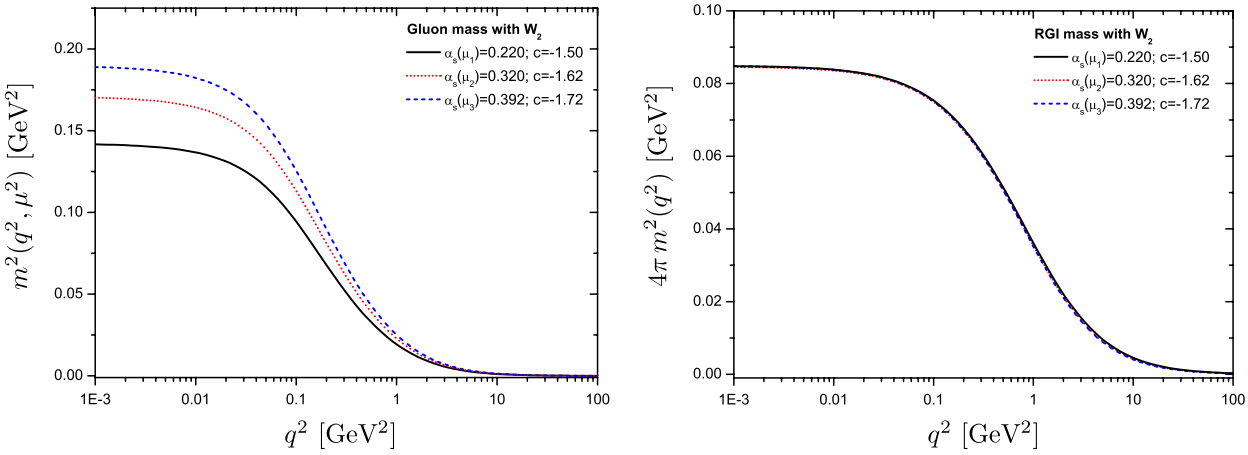

FIG. 9 (color online). The numerical solution for $m^2(q^2,\mu^2)$ (left panel) using the model of Eq. (6.7) for the three renormalization scales μ_i; the corresponding RGI mass $4\pi\bar{m}^2(q^2)$ given by Eq. (2.30) is shown on the right panel.

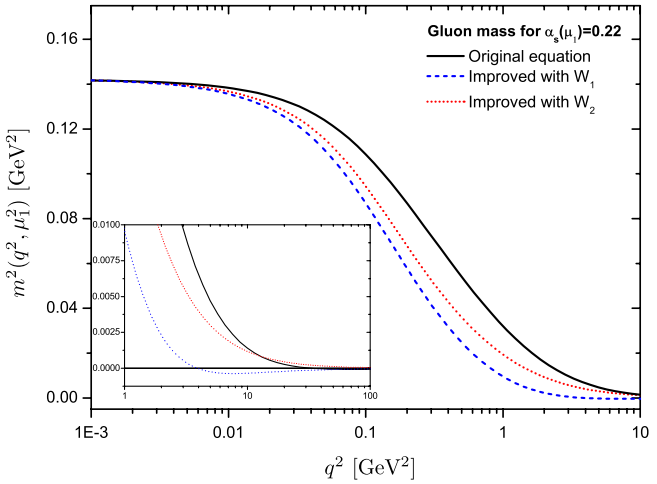

FIG. 10 (color online). Comparison of the numerical results obtained for $m^2(q^2,\mu_1^2)$ using the original gluon mass equation (black continuous); the improved versions with W_1 of Eq. (6.6) (blue dashed) and W_2 of Eq. (6.7) (red dotted). The inset shows a zoom in the UV tail of the same quantities.

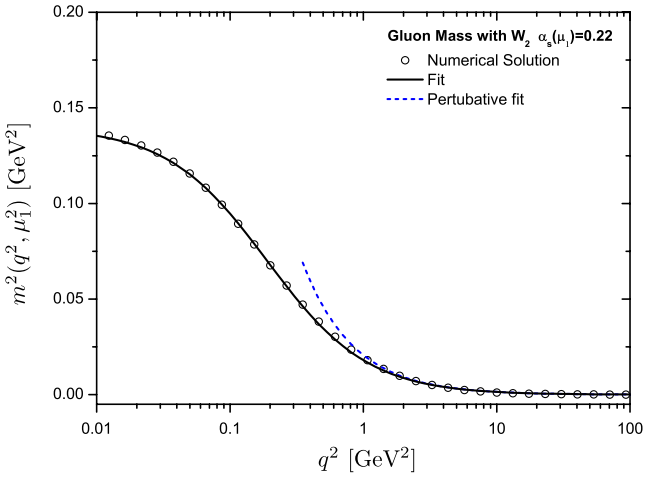

FIG. 11 (color online). The numerical solution for $m^2(q^2)$ obtained using the RG-improved Ansatz W_2 of Eq. (6.7) (black circles). The (black) continuous curve represents the fit of Eq. (6.9) while the (blue) dashed curve is the asymptotic fit for the ultraviolet tail given by Eq. (6.10).

unique curve. In fact, the less favorable point is located at $q^2 \approx 25$ GeV^2, where the relative error is around 10%. In addition, the solutions obtained with W_2 remain positive and monotonically decreasing through the *entire range* of physical momenta. For the curves presented in Eq. (6.7), we have chosen $c = -1.50$ for μ_1, $c = -1.62$ for μ_2, and $c = -1.72$ for μ_3.

In Fig. 10 we compare the numerical solutions for $m^2(q^2,\mu_1^2)$ obtained from the three different models. The solution of the original version of the gluon mass equation is represented by the (black) continuous curve, while the solutions using Eq. (6.6) and Eq. (6.7) are indicated by (blue) dashed and (red) dotted curves, respectively. When the gluon propagator is renormalized at the point μ_1, its saturation value in the deep IR is given by

$$\Delta^{-1}(0) = 0.14 \text{ GeV}^2 = m^2(0) \equiv m_0^2. \tag{6.8}$$

Therefore, the three masses coincide at the origin, i.e., $m_0 = 375$ MeV. However, in the intermediate region, we clearly see differences in their momentum dependence. Notice that, in this particular region, the original equation produces a $m^2(q^2)$ that falls off slower than the improved versions. On the other hand, the $m^2(q^2)$ obtained with the W_1 decreases considerably faster than the other two cases. The UV tails of these solutions are shown separately in the insert; as already mentioned, only the one originating from Eq. (6.7) stays strictly positive for all momenta.

C. Physically motivated fit

It turns out that the three different masses in Fig. 10 may be fitted very accurately by a single, particularly simple function, namely,

$$m^2(q^2) = \frac{m_0^2}{1 + (q^2/\mathcal{M}^2)^{1+p}}. \tag{6.9}$$

The corresponding sets of optimal values, $(\mathcal{M}, p)$, for the mass scale $\mathcal{M}$ and the exponent p are as follows: (i) (557 MeV, 0.08) for the black continuous curve, (ii) (381 MeV, 0.26) for the blue dashed curve, and (iii) (436 MeV, 0.15) for the red dotted curve. All fits have a reduced $\chi^2 \approx 0.99$. Note that $\mathcal{M}$ is just a dimensionful fitting parameter, not to be confused with the characteristic QCD mass scale, Λ; in fact, within the MOM scheme that we use, and for $\alpha_s = 0.22$, we have that $\Lambda_{\rm MOM} = 280$ MeV [73].

To appreciate the quality of the above fit, in Fig. 11 we superimpose the numerical solution for the RG-improved Ansatz W_2 when $\alpha(\mu_1) = 0.22$ (black circles) and the fit of Eq. (6.9) (black continuous curve). Clearly, the coincidence between the two curves is striking.

Let us now take a closer look at the asymptotic form of $m^2(q^2)$ for large q^2, to be denoted by $m^2_{\rm UV}(q^2)$. From Eq. (6.9) it is clear that, for sufficiently large values of q^2, the 1 may be depreciated in the denominator of Eq. (6.9), yielding

$$m^2_{\rm UV}(q^2) = \frac{m_0^2\Lambda^2}{q^2}(q^2/\mathcal{M}^2)^{-p}. \tag{6.10}$$

As is shown in Fig. 11, the onset of the asymptotic form (6.10) is clear already at momenta of the order of a few GeV.

The particular asymptotic behavior described in Eq. (6.10) corresponds precisely to the so-called "power-law" running of the effective gluon mass, first conjectured in Ref. [74] and subsequently studied in Refs. [75,76]. Its

main physical implication is that the condensates of dimension 2 do not contribute to the OPE expansion of $m^2_{\rm UV}(q^2)$ because otherwise the corresponding running would be logarithmic. Then, in the absence of quarks, the lowest-order condensates appearing in the OPE of the mass are those of dimension 4, namely, the (gauge-invariant) $\langle 0|: G^a_{\mu\nu}G^{\mu\nu}_a : |0\rangle$, and possibly the ghost condensate $\langle 0|: \bar{c}^a \Box c^a : |0\rangle$ [77,78]. Since, on dimensional grounds, these condensates must be divided by q^2, one obtains (up to logarithms) the aforementioned power-law running for the mass.

It remains to be seen if Eq. (6.10) is a fortuitous coincidence related to a particular Ansatz for the kernel (namely, W_2) or if it really reflects an intrinsic feature of the gluon mass.

D. Comparison with related studies

Since the advent of the the concept of a dynamical gluon mass [19], a multitude of field-theoretic and phenomenological studies has placed bounds or provided estimates for this particular quantity. However, in general, a direct comparison of all such results ought to be carried out with particular care, especially since, in addition to the vast methodological differences underlying several of these works, the very definition and meaning of the term "gluon mass" has not yet reached a global consensus. Nonetheless, it is a useful exercise to go over some representative examples, if only for the purpose of checking whether the values obtained in each case are reasonably compatible with each other.

To begin with, one should notice that, even within the PT-BFM formalism that we employ, the issue of the gauge dependence is expected to cause deviations to the final results. For example, the original work of Ref. [19], which in modern language would correspond to the Feynman gauge of the BFM, yielded $m \sim 500 \pm 200$ MeV; instead, in the present work, the Landau gauge is used, producing the range of masses $375 - 434$ MeV. These latter values lie within the range proposed in Ref. [19], albeit toward the low range of the interval.

A different approach was presented in Ref. [86], where an estimate of the effective gluon mass was obtained through a detailed study of the low-momentum behavior of the (Landau gauge) ghost dressing function and its subsequent comparison with data originating from big lattice simulations. The main idea may be summarized as follows. A massive gluon propagator of the form $(q^2 + m_0^2)^{-1}$ has been inserted into the SDE that controls the momentum evolution of $F(q^2)$; evidently, the presence of the gluon mass mass saturates $F(q^2)$ in the IR, in accordance with the general qualitative lattice observations. The $F(q^2)$ so obtained is then fitted to various sets of $SU(3)$ lattice data, including those of Ref. [30] that we have used here. The final result of $m_0 \sim 500$ MeV appears to be in rather good agreement with those obtained here, especially in view of the variety of (not necessarily equivalent) approximations employed in both works, and the differences in some of the lattice data employed.

TABLE I. An indicative collection of gluon mass scale estimates available in the literature.

Gluon mass scale [MeV]	Method	Reference
$300 \div 700$	SDEs	[19]
600	Lattice	[79]
$500 \div 800$	Phenomenology	[80–82]
$570 \div 750$	Lattice	[83]
370	Lattice	[24]
$400 \div 600$	Lattice	[84]
$650 \div 700$	Lattice	[85]
500	SDEs + lattice	[86]
$600 \div 700$	SDEs	[87]
$375 \div 434$	SDEs + lattice	This work

In Ref. [87] the gluon and ghost SDEs were integrated in the full complex momentum plane, which allowed the construction of the gluon spectral function. The location of the positive peak of the latter function served as a definition of an effective gluon mass m_g, with $m_g \in [600, 700]$ MeV.

Many other methods have been used to provide estimates of this quantity, including hadron phenomenology [80–82] and, obviously, the lattice [24,79,83–85]. For the convenience of the reader, we report in Table I the estimates obtained in these papers. Even though, as already mentioned, the meaningful interpretation of these numbers is rather subtle, they do seem to convey a sense of underlying consistency.

E. Massive gluons and glueball masses

In the absence of quarks, the physical spectrum of Yang–Mills theories consists of color-less composite states made out of gluon fields, known as glueballs [88] (for a recent review, see Ref. [89]). Therefore, even though the gluon masses reported here depend on the gauge choice (Landau gauge) and the renormalization point, one would expect a systematic way of relating them to the physical glueball masses. However, to date, such a fundamental relation eludes us. In this subsection we present a brief account of the general field-theoretic procedures used for computing the glueball masses and comment on some of the technical difficulties and theoretical uncertainties involved.

It would certainly seem a natural starting point to treat glueballs as nonrelativistic bound states, consisting of either two or three gluons, in a direct analogy to mesons and baryons, respectively. Within such a framework, the relative lightness of the gluon masses found here (of about 400 MeV) would appear difficult to reconcile with quenched lattice studies [90], which place the mass of the lowest 0^{++} glueball state in the range of 1.7 GeV. This difficulty became apparent already in the classic work by Cornwall and Soni [91], where a screened potential [92]

was used as input into the corresponding Schrödinger equation, yielding a lowest (scalar) glueball mass around 1.3 GeV, for an effective gluon mass of about 500 MeV. However, as explicitly cautioned in the aforementioned work, a nonrelativistic treatment may be marginally compatible with such a (light) gluon mass, and a more sophisticated relativistic approach may be instead required.

The prime candidate for such a fundamental approach is provided by the Bethe–Salpeter equations (BSEs), which form a system of nonperturbative integral equations for the bound states of the theory, derived through formal manipulations of the generating functional of the theory. In fact, these equations bear a strong theoretical kinship to the SDEs that control the dynamics of the off-shell Green's functions [1] and constitute the natural way for relating the gluon mass (derived from the SDE) with the glueball masses (obtained from the BSE). Actually, there exists a strong interplay between both types of equations: since the kernel of the BSE is in general composed by off-shell Green's functions, the nonperturbative information obtained from the SDEs for the latter represents a crucial ingredient for the former [93–95].

A typical BSE describing a glueball is a homogeneous integral equation of the Fredholm type, which is diagrammatically depicted in Fig. 12. From such an equation, one may obtain, at least in principle, the so-called Bethe–Salpeter (BS) wave functions and the position of the bound states masses. Specifically, the determination of the masses is basically reduced to solving a functional eigenvalue problem.

To see in some detail how this works, one must first decompose the BS amplitude, $\chi_{\mu\nu}$, in the most general scalar, pseudoscalar, or tensorial basis, depending on the total spin of the glueball under consideration. Then, the relevant form factors, which respect the parity constraints of the bound-state under study, can be selected using appropriate projectors. The resulting equation corresponds to an eigenvalue problem (in Euclidean space) of the type

$$\mathcal{F}(P^2,q^2,P\cdot q)=\lambda(P^2)\int_k \mathcal{K}_1(P^2,q^2,k^2,P\cdot q,P\cdot k)\cdot\mathcal{F}(P^2,q^2,P\cdot k), \tag{6.11}$$

where P is the total momentum of the glueball, q is the relative momentum, and k is the loop momentum. Note that a multiplicative free parameter, $\lambda(P^2)$, has been introduced on the rhs of Eq. (6.11); the original BSE will be recovered only when $\lambda(P^2)=1$. In addition, it is easy to appreciate that the eigenvectors and eigenvalues, obtained as solutions of Eq. (6.11), depend on the glueball momentum P^2.

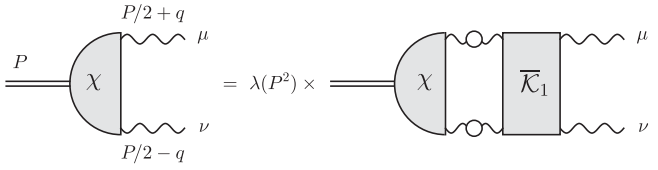

FIG. 12. Schematic representation of a gluonic BSE.

Then, computing Eq. (6.11) for different values of P^2, one can find that, for a particular value of P^2, the eigenvalue will become $\lambda(P^2=-M_{gb}^2)=1$. This special value, M_{gb}^2, is identified with the mass of the glueball bound state. It is important to stress that, due to the presence of the scalar products $P\cdot q$ and $P\cdot k$ in the kernel of the BSE, the above integration probes parts of the complex momentum plane. Therefore, in general, it is necessary to know the structure of some of the relevant Green's function also in the Minkowski region.

It must be clear from the above discussion, and the intrinsic complexity of the equations involved in this formalism, that the IR value of the gluon mass and the corresponding M_{gb}^2 are very difficult to correlate. In fact, it is rather likely that the relevant integration region, namely, the one that provides the largest support to the BSE, is not the deep IR but rather the intermediate momentum scales of order $0.3\div 1$ GeV. In such a case, the determining factor is the support of the gluon propagator in the aforementioned momentum region rather than its value at $q^2=0$. For instance, the gluon propagator obtained on the lattice and a simple "massive" propagator of the form $(q^2+m_0^2)^{-1}$ [recall Eq. (6.8)] may coincide at $q^2=0$ (i.e., have the same IR gluon "mass"), but the former is significantly more enhanced for intermediate momenta, as shown in Fig. 13. This enhancement, in turn, is known to have important quantitative implications in the context of nonlinear integral equations [1,6,37].

Recently, a first attempt to compute glueball masses within the BSE formalism was presented in Ref. [96]. Using a series of approximations for all Green's functions

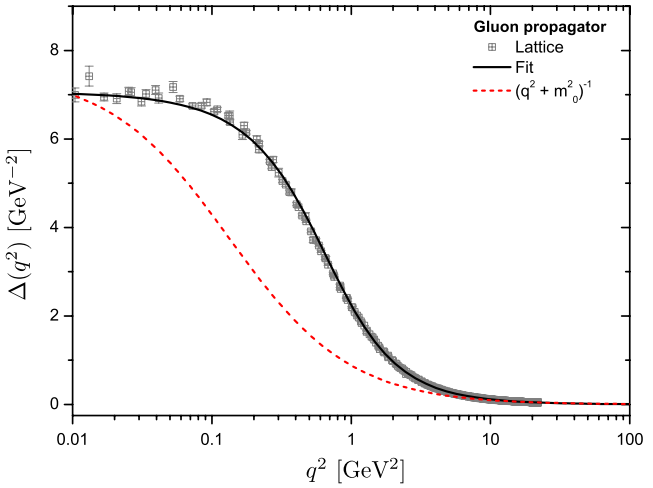

FIG. 13 (color online). Comparison of the lattice data for the gluon propagator for $\mu_1=4.3$ GeV (black continuous) with the simple massive gluon propagator with $m_0^2=0.14$ GeV^2 (red dashed). Lattice data are taken from Ref. [30].

entering into the BSE kernel, a reasonably good spectrum was obtained, with the mass for the scalar glueball, 0^{++}, around 1.75 GeV and that of the pseudoscalar state, 0^{-+}, around 2.75 GeV. Despite this positive outcome, as the authors of Ref. [96] pointed out, the spectrum appears to be particularly sensitive to the approximations employed for the BSE kernel. Therefore, further systematic work is required in order to place the entire picture on a firm theoretical basis.

VII. DISCUSSION AND CONCLUSIONS

In this work we have presented a detailed study of the RG structure of the integral equation that controls the dynamical evolution of the gluon mass. Specifically, we have shown that the renormalization of this equation can be carried out entirely by means of the renormalization constants employed in the standard perturbative treatment, namely, those associated with the gluon and ghost wave functions and the fundamental vertices of the theory. In addition, by making explicit use of the diagrammatic equivalence between the skeleton expansion of the three gluon vertex in the SDE and BS formalisms, the kernel of the gluon mass equation can be written exclusively in terms of the renormalized Green's functions, with no reference to any cutoff-dependent renormalization constants [see Eq. (3.10)].

The RG properties of the full mass equation are inevitably distorted when approximate expressions are used for its kernel. The departure of the solutions from the correct RG behavior is quantitatively described in terms of the RGI gluon mass, $\bar{m}^2(q^2)$, and can serve as a discriminant for the various Ansätze employed for the kernel. Using this criterion, we have established that the $\bar{m}^2(q^2)$, constructed using as input the solution $m^2(q^2)$ obtained from the original version of the mass equation [21], deviates considerably from the optimal RGI behavior (see Fig. 7).

Then, motivated by the RG properties that the kernel must satisfy, two new versions of the gluon mass equation were put forth [see Eqs. (6.6) and (6.7)], which are expected to display an improved RG behavior. Indeed, our numerical analysis reveals that the $\bar{m}^2(q^2)$ obtained from both RG-improved Ansätze capture more faithfully the RG properties of the exact equation. Specifically, the deviations between the $\bar{m}^2(q^2)$ obtained for different μ's displays, in the less favorable regions, relative errors around 12% and 10%, respectively. In addition, and contrary to the other two cases, the Ansatz of Eq. (6.7) presents a well-defined positive UV tail in all range of momenta. We therefore conclude that, overall, the best available functional form for the kernel is given by Eq. (6.7).

Interestingly enough, W_2 has a simpler structure than W_1, in the sense that it contains a single adjustable parameter instead of two, and yet it produces results that are in better compliance with the basic theoretical principles that we have considered. The reason for that may be related to the overall sign of the gluon mass equations, and the degree at which each Ansatz succeeds to effectively reverse it. Specifically, as already mentioned after Eq. (5.7), the negative sign on the rhs of Eq. (4.9) must be compensated by negative contributions coming from the kernel. In the case of W_2, this is accomplished directly, and in a rather elementary way, because the parameter c is simply chosen such that $1 + c$ becomes sufficiently negative. Instead, W_1 performs the same task in a less efficient way, which may be reflected in the slightly enhanced departure of the resulting mass from the perfect RG invariance and the change of its sign in the deep UV.

It is clear that a more rigorous determination of the kernel is required in order to further substantiate our analysis. It is worth pointing out that, in this effort, one may want to keep open the possibility of working with the lhs of Eq. (3.8), rather than its rhs. Indeed, whereas for the formal demonstration presented in Sec. III the rhs of Eq. (3.8) seems to be advantageous, because it is free of the renormalization constants Z, for the actual computation of $\mathcal{G}^{\mu\alpha\beta}$, the lhs may turn out to be easier to handle. Of course, in order to make progress with the lhs, in addition to obtaining a better approximation for the quantity $Y(k)$, one ought to provide appropriate expressions for the renormalization constants Z. These tasks are technically particularly subtle and laborious because they require, among other things, a tight control on the structure of the various fully dressed vertices of the theory. In fact, the multiplicative renormalizability and the correct cancellation of overlapping divergences depends crucially on the detailed knowledge of the transverse (automatically conserved) part of the corresponding vertex (in our case of the three-gluon vertex), which forces one to go beyond the usual gauge-technique-inspired Ansätze for the vertex in question [3]. These difficulties have been exemplified, and only partially circumvented, in the studies of the gap equation that controls the chiral symmetry breaking and the dynamical generation of a constituent quark mass [1–3,37]. We hope to make progress on some of these issues in future works.

ACKNOWLEDGMENTS

The research of J. P. is supported by the Spanish MEYC under Grant No. FPA2011-23596. The research of A. C. A is supported by the National Council for Scientific and Technological Development—CNPq under Grant No. 306537/2012-5 and Project No. 473260/2012-3 and by São Paulo Research Foundation—FAPESP through Project No. 2012/15643-1.

[1] C. D. Roberts and A. G. Williams, Prog. Part. Nucl. Phys. **33**, 477 (1994).
[2] D. C. Curtis and M. R. Pennington, Phys. Rev. D **48**, 4933 (1993).
[3] A. Kizilersu and M. Pennington, Phys. Rev. D **79**, 125020 (2009).
[4] P. Boucaud, J. P. Leroy, A. L. Yaouanc, J. Micheli, O. Pène, and J. Rodríguez-Quintero, J. High Energy Phys. 06 (2008) 012.
[5] P. Boucaud, J. P. Leroy, A. L. Yaouanc, J. Micheli, O. Pène, and J. Rodríguez-Quintero, J. High Energy Phys. 06 (2008) 099.
[6] R. Alkofer and L. von Smekal, Phys. Rep. **353**, 281 (2001).
[7] C. S. Fischer, J. Phys. G **32**, R253 (2006).
[8] A. P. Szczepaniak, Phys. Rev. D **69**, 074031 (2004).
[9] A. P. Szczepaniak and E. S. Swanson, Phys. Rev. D **65**, 025012 (2001).
[10] A. C. Aguilar and J. Papavassiliou, J. High Energy Phys. 12 (2006) 012.
[11] A. Aguilar, D. Binosi, and J. Papavassiliou, Phys. Rev. D **78**, 025010 (2008).
[12] M. Pennington and D. Wilson, Phys. Rev. D **84**, 119901 (2011).
[13] M. Q. Huber and L. von Smekal, J. High Energy Phys. 04 (2013) 149.
[14] D. R. Campagnari and H. Reinhardt, Phys. Lett. B **707**, 216 (2012).
[15] A. P. Szczepaniak and H. Reinhardt, Phys. Rev. D **84**, 056011 (2011).
[16] J. M. Pawlowski, Ann. Phys. (Amsterdam) **322**, 2831 (2007).
[17] J. M. Pawlowski, D. F. Litim, S. Nedelko, and L. von Smekal, Phys. Rev. Lett. **93**, 152002 (2004).
[18] C. Popovici, P. Watson, and H. Reinhardt, *Proc. Sci.* (2011) 036.
[19] J. M. Cornwall, Phys. Rev. D **26**, 1453 (1982).
[20] A. Aguilar, D. Binosi, and J. Papavassiliou, Phys. Rev. D **84**, 085026 (2011).
[21] D. Binosi, D. Ibanez, and J. Papavassiliou, Phys. Rev. D **86**, 085033 (2012).
[22] A. Aguilar, D. Binosi, and J. Papavassiliou, Phys. Rev. D **88**, 074010 (2013).
[23] V. Nair, Phys. Rev. D **88**, 105027 (2013).
[24] O. Philipsen, Nucl. Phys. **B628**, 167 (2002).
[25] A. C. Aguilar, A. A. Natale, and P. S. Rodrigues da Silva, Phys. Rev. Lett. **90**, 152001 (2003).
[26] A. C. Aguilar, A. Mihara, and A. A. Natale, Phys. Rev. D **65**, 054011 (2002).
[27] A. Aguilar, D. Binosi, J. Papavassiliou, and J. Rodriguez-Quintero, Phys. Rev. D **80**, 085018 (2009).
[28] D. Dudal, J. A. Gracey, S. P. Sorella, N. Vandersickel, and H. Verschelde, Phys. Rev. D **78**, 065047 (2008).
[29] A. Cucchieri and T. Mendes, *Proc. Sci.* LAT2007 (2007), 297.
[30] I. Bogolubsky, E. Ilgenfritz, M. Muller-Preussker, and A. Sternbeck, Phys. Lett. B **676**, 69 (2009).
[31] O. Oliveira and P. Silva, *Proc. Sci.* QCD-TNT09 (2009), 033.
[32] P. O. Bowman, U. Heller, D. Leinweber, M. Parappilly, A. Sternbeck, L. von Smekal, A. Williams, and J. Zhang, Phys. Rev. D **76**, 094505 (2007).
[33] A. Ayala, A. Bashir, D. Binosi, M. Cristoforetti, and J. Rodriguez-Quintero, Phys. Rev. D **86**, 074512 (2012).
[34] C. S. Fischer and R. Alkofer, Phys. Rev. D **67**, 094020 (2003).
[35] J. Papavassiliou and J. M. Cornwall, Phys. Rev. D **44**, 1285 (1991).
[36] A. G. Williams, G. Krein, and C. D. Roberts, Ann. Phys. (N.Y.) **210**, 464 (1991).
[37] A. Aguilar and J. Papavassiliou, Phys. Rev. D **83**, 014013 (2011).
[38] D. August and A. Maas, J. High Energy Phys. 07 (2013) 001.
[39] J. D. Bjorken and S. Drell, *Relativistic Quantum Fields* (Mcgraw-Hill, New York, 1979).
[40] R. Jackiw and K. Johnson, Phys. Rev. D **8**, 2386 (1973).
[41] R. Jackiw, in *Erice 1973, Proceedings, Laws of Hadronic Matter, New York, 1975*, pp. 225–251.
[42] J. M. Cornwall and R. E. Norton, Phys. Rev. D **8**, 3338 (1973).
[43] E. Eichten and F. Feinberg, Phys. Rev. D **10**, 3254 (1974).
[44] E. C. Poggio, E. Tomboulis, and S. H. H. Tye, Phys. Rev. D **11**, 2839 (1975).
[45] J. S. Schwinger, Phys. Rev. **125**, 397 (1962).
[46] J. S. Schwinger, Phys. Rev. **128**, 2425 (1962).
[47] A. C. Aguilar and J. Papavassiliou, Phys. Rev. D **81**, 034003 (2010).
[48] K. G. Wilson, Phys. Rev. **179**, 1499 (1969).
[49] M. A. Shifman, A. I. Vainshtein, and V. I. Zakharov, Nucl. Phys. **B147**, 385 (1979).
[50] M. A. Shifman, A. I. Vainshtein, and V. I. Zakharov, Nucl. Phys. **B147**, 448 (1979).
[51] J. M. Cornwall and J. Papavassiliou, Phys. Rev. D **40**, 3474 (1989).
[52] A. Pilaftsis, Nucl. Phys. **B487**, 467 (1997).
[53] D. Binosi and J. Papavassiliou, Phys. Rev. D **66**, 111901(R) (2002).
[54] D. Binosi and J. Papavassiliou, J. Phys. G **30**, 203 (2004).
[55] D. Binosi and J. Papavassiliou, Phys. Rep. **479**, 1 (2009).
[56] L. F. Abbott, Nucl. Phys. **B185**, 189 (1981).
[57] D. Binosi and J. Papavassiliou, Phys. Rev. D **77**, 061702 (2008).
[58] D. Binosi and J. Papavassiliou, J. High Energy Phys. 11 (2008) 063.
[59] P. A. Grassi, T. Hurth, and M. Steinhauser, Ann. Phys. (N.Y.) **288**, 197 (2001).
[60] D. Binosi and J. Papavassiliou, Phys. Rev. D **66**, 025024 (2002).
[61] A. Aguilar, D. Binosi, and J. Papavassiliou, J. High Energy Phys. 11 (2009) 066.
[62] P. A. Grassi, T. Hurth, and A. Quadri, Phys. Rev. D **70**, 105014 (2004).
[63] A. Aguilar, D. Binosi, and J. Papavassiliou, J. High Energy Phys. 07 (2010) 002.
[64] P. Pascual and R. Tarrach, Lect. Notes Phys. **194**, 1 (1984).
[65] A. Aguilar, D. Ibanez, V. Mathieu, and J. Papavassiliou, Phys. Rev. D **85**, 014018 (2012).
[66] D. Ibañez and J. Papavassiliou, Phys. Rev. D **87**, 034008 (2013).
[67] D. Binosi, D. Ibanez, and J. Papavassiliou, Phys. Rev. D **87**, 125026 (2013).

[68] A. Aguilar, D. Binosi, D. Ibañez, and J. Papavassiliou, arXiv:1312.1212.
[69] J. S. Ball and T.-W. Chiu, Phys. Rev. D **22**, 2542 (1980).
[70] B. Holdom, Phys. Lett. B **728**, 467 (2014).
[71] A. Aguilar, D. Binosi, and J. Papavassiliou, Phys. Rev. D **86**, 014032 (2012).
[72] A. Aguilar, D. Ibáñez, and J. Papavassiliou, Phys. Rev. D **87**, 114020 (2013).
[73] P. Boucaud, F. De Soto, J. Leroy, A. L. Yaouanc, J. Micheli, O. Pène, and J. Rodríguez-Quintero, Phys. Rev. D **79**, 014508 (2009).
[74] J. M. Cornwall and W.-S. Hou, Phys. Rev. D **34**, 585 (1986).
[75] M. Lavelle, Phys. Rev. D **44**, R26 (1991).
[76] A. C. Aguilar and J. Papavassiliou, Eur. Phys. J. A **35**, 189 (2008).
[77] M. J. Lavelle and M. Schaden, Phys. Lett. B **208**, 297 (1988).
[78] E. Bagan and T. G. Steele, Phys. Lett. B **219**, 497 (1989).
[79] J. E. Mandula and M. Ogilvie, Phys. Lett. B **185**, 127 (1987).
[80] G. Parisi and R. Petronzio, Phys. Lett. B **94**, 51 (1980).
[81] F. Halzen, G. I. Krein, and A. A. Natale, Phys. Rev. D **47**, 295 (1993).
[82] M. B. Gay Ducati, F. Halzen, and A. A. Natale, Phys. Rev. D **48**, 2324 (1993).
[83] C. Alexandrou, P. de Forcrand, and E. Follana, Phys. Rev. D **65**, 114508 (2002).
[84] T. Iritani, H. Suganuma, and H. Iida, Phys. Rev. D **80**, 114505 (2009).
[85] O. Oliveira and P. Bicudo, J. Phys. G **38**, 045003 (2011).
[86] P. Boucaud, M. E. Gómez, J. P. Leroy, A. Le Yaouanc, J. Micheli, O. Pène, and J. Rodríguez-Quintero, Phys. Rev. D **82**, 054007 (2010).
[87] S. Strauss, C. S. Fischer, and C. Kellermann, Phys. Rev. Lett. **109**, 252001 (2012).
[88] H. Fritzsch and P. Minkowski, Nuovo Cim. A **30**, 393 (1975).
[89] V. Mathieu, N. Kochelev, and V. Vento, Int. J. Mod. Phys. E **18**, 1 (2009).
[90] C. J. Morningstar and M. J. Peardon, Phys. Rev. D **60**, 034509 (1999).
[91] J. M. Cornwall and A. Soni, Phys. Lett. B **120**, 431 (1983).
[92] C. W. Bernard, Phys. Lett. B **108**, 431 (1982).
[93] P. Maris and C. D. Roberts, Int. J. Mod. Phys. E **12**, 297 (2003).
[94] L. Chang, C. D. Roberts, and P. C. Tandy, Chin. J. Phys. **49**, 955 (2011).
[95] G. Eichmann, J. Phys. Conf. Ser. **426**, 012014 (2013).
[96] J. Meyers and E. S. Swanson, Phys. Rev. D **87**, 036009 (2013).